Critical Review of the Effect of Water Saturation Variation on Pore Pressure Estimation Technique

by

Yslam Sahetmyradov
(G02349)

Dissertation submitted in partial fulfilment of
the requirements for the
MSc. Petroleum Engineering
(MSc. PE)

JULY 2014

Universiti Teknologi PETRONAS
31750 Bandar Seri Iskandar
Perak Darul Ridzuan

CERTIFICATION OF APPROVAL

Critical Review of the Effect of Water Saturation Variation on Pore Pressure Estimation Technique

by

Yslam Sahetmyradov
(G02349)

A project dissertation submitted to the
Petroleum Engineering Programme
Universiti Teknologi PETRONAS
in partial fulfilment of the requirement for the
MSc. of PETROLEUM ENGINEERING

Approved by,

_____

(Dr. Masoud Rashidi)

Universiti Teknologi PETRONAS
31750 Bandar Seri Iskandar
Perak Darul Ridzuan

July 2014

CERTIFICATION OF ORIGINALITY

This is to certify that I am responsible for the work submitted in this project, that the original work is my own except as specified in the references and acknowledgements, and that the original work contained herein have not been undertaken or done by unspecified sources or persons.

_____

YSLAM SAHETMYRADOV
(G02349)

ABSTRACT

Pore pressure estimation is a critical process in terms of safety and economy of time and money during exploration, drilling and production operations. The knowledge of pore pressure gradients is invaluable in modelling correct mud weights and designing casing configuration for well construction. The properly estimated pore pressure gradients allow avoiding, or at least mitigating, the risks associated with drilling such as pressure kicks, well blowouts, formation damage and loss of circulation. Conventional well-log based methods of pore pressure prediction convert porosity indicators, such as sonic travel time/velocity and resistivity, into pore pressure estimates. The methods are developed in application to normal water bearing shale with 100% water saturation. This research study reviewed the effect of gas presence and associated water saturation variation in unconventional shale gas formations on conventional pore-pressure estimation technique, as well as on workflow of pore pressure analysis. The review of previous publications discovered that: (a) in normal shale, water saturation always equals unity and it does not affect a pore-pressure estimation technique; (b) in unconventional shale gas formations, water saturation alteration, through the gas presence, indirectly affects the pore-pressure estimation technique reducing its accuracy of prediction. Particularly, it causes the sonic compressional velocity (V_p) to be slower / transit time (Δt_c) to increase. However, strictly speaking, the original cause of this effect is the gas presence, and water saturation alteration is associated with the gas saturation ($S_w = 1 - S_g$). To correct the gas effect on compressional velocity (V_p), a downhole measured shear velocity (V_s) should be used due to its low response to gas in porous medium. The method using corrected compressional velocity is applicable to predict pore pressure both in unconventional shale gas formations and in gas-bearing formations in conventional reservoirs. The inspection of correlation between water saturation and pore pressure, calculated after the correction of gas effect, in such kind of reservoir as shale gas formation, following the proposed methodology, was given as a recommendation for future project work.

ACKNOWLEDGEMENTS

I would like to express my deepest gratitude and acknowledgement to:

1) Dr. Masoud Rashidi - Project Supervisor and Senior Lecturer, Programme Manager in MSc in Petroleum Engineering by Coursework and Dissertation at the Universiti Teknologi PETRONAS – for his supervision, assistance and constructive criticism in writing this project.
2) Mr. Saleem Qadir Tunio - Individual Project Coordinator at Universiti Teknologi PETRONAS – for his briefing on Individual Project and other given details.
3) Lecturers and members during the course of study in MSc in Petroleum Engineering from Universiti Teknologi PETRONAS and Heriot-Watt University for their instructions and helps.

TABLE OF CONTENTS

LIST OF FIGURES

LIST OF TABLES

ABBREVIATIONS

EqMW = Equivalent Mud Weight

NCT = Normal Compaction Trend

NMR = Nuclear Magnetic Resonance

PPM = Parts Per Million

TOC = Total Organic Carbon

TVD = True Vertical Depth

CHAPTER 1
INTRODUCTION

1.1 BACKGROUND

Pore pressure or formation pressure (P_p) is the pressure exerted by the fluid contained within a pore space of formation [1]. If the pore pressure is lower or higher than the hydrostatic pressure (P_{hyd}) (normal pore pressure), it is abnormal pore pressure. When pore pressure exceeds the normal pressure, it is overpressure (or surpressure), whereas pore pressure less than hydrostatic pressure, it is underpressure (subpressure) [2].

Detection and quantitative estimation of abnormally pressured formations are crucial to exploration, drilling, and production activities [2]. Uncertainties of pore pressure, particularly of overpressure, can significantly increase drilling non-productive time and cause serious drilling incidents such as stuck pipes, formation damage, fluid flux, wellbore instability, pressure kicks and well blowouts [3] [4].

Although underpressure is not always given the same attention as overpressure, but entering such intervals with an overbalanced mud system can definitely cause problems such as mud invasion, formation damage and fracture, loss of circulation and hydrostatic control [1].

All these incidents may lead to loss of time, money and even human lives.

Therefore, awareness of pore pressure in combination with fracture gradients is the basis for economically and safely drilling wells with correctly programmed mud weights, properly designed casing configuration (casing sizes and setting depths), and efficient well completions, and allow for killing the well in case of fluid influx without fracturing

formations in open hole section [2]. Figure 1 presents the example of how pore pressure and fracture gradients can be used to select casing setting depths. Casing shoes are set below the formation breakdown points.

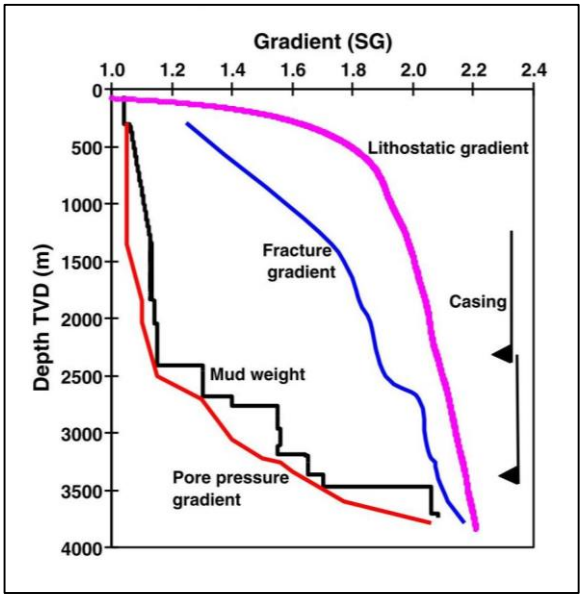

Fig. 1.1. Pore pressure gradient, fracture gradient, overburden stress gradient (lithostatic gradient), mud weight, and casing shoes with depth [3].

Overpressures can be generated by a variety of mechanisms among which are:

a) Overburden effect (undercompaction)
b) Tectonic stresses (lateral stresses, uplift, faulting or folding of rocks)
c) Increases in fluid volume (water release due to clay diagenesis and gypsum dehydration, hydrocarbon generation and gas cracking, aquathermal expansion)
d) Osmosis (water flow from less saline or fresh water formation to more saline water formation resulting in pressure discharging and charging, respectively)
e) Hydrostatic effects (hydraulic head and hydrocarbon buoyancy)

Before a reliable analysis of pore pressure commenced, many sources of data have to be considered and evaluated. Quite often, different sources of data give conflicting results about pore pressure alteration, and engineer has to estimate which sources are relevant and reliable [1].

Pore pressure analyses consists of three categories: pre-drill pore pressure prediction, pore pressure prediction while drilling and post-well pore pressure analysis. The pre-drill pore pressure analyses, as an initial source, uses the seismic interval velocity data in the planned well location, regional geology data, well logging and drilling data in the offset wells. The pore pressure prediction while drilling generally uses the logging while drilling (LWD), measurement while drilling (MWD), drilling parameters, and mud logging data for analyses. The post-well analysis in the drilled wells deal with all available data to build pore pressure model, which can be used for pre-drill pore pressure estimations for future drilling programs [3]. Fig. 2 presents a workflow for pore pressure analyses using all available data.

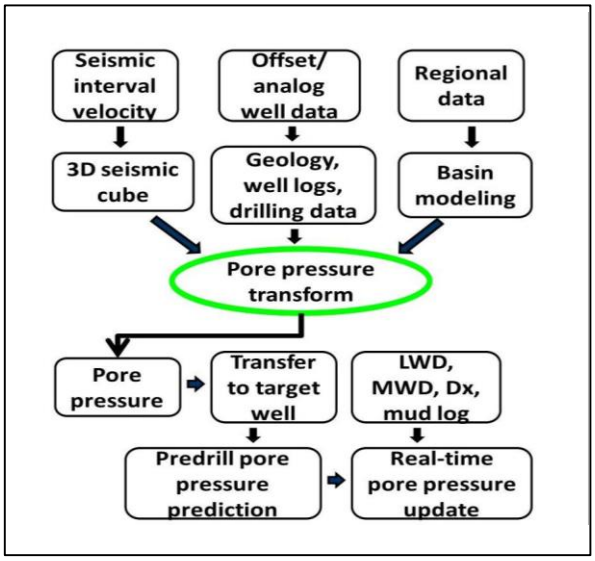

Fig. 1.2. Schematic workflow for pore pressure analysis [5].

In this report, exactly the well logging data from offset wells only were considered as a technique for pre-drill pore pressure prediction in future wells. Well-log based methods of pore pressure estimation are based on the shale (mudrock) properties. The pore pressures obtained from these methods are the pressures in shale. Pore pressures in permeable formations (sandstone, limestone) are estimated referring to pressures in shale [3]. Well-log based methods of pore pressure prediction convert porosity indicators, such as sonic travel time/velocity and resistivity, into pore pressure estimates [4].

1.2 PROBLEM STATEMENT

The ability to estimate pore pressure is vital in terms of safety and economy of time and money during exploration, drilling and production operations [2]. The knowledge of pore pressure gradients is invaluable in modelling correct mud weights and casing programs.

Whatever the mechanism causes formation overpressured, what all of them have in common is that the zone in question contains an abnormal (excessive) volume of formation fluid due to inability of the retained fluids to escape at sufficient rate to maintain a pore pressure (P_p) in equilibrium with normal hydrostatic pressure (P_{hyd}) of the region [1] [6]. Therefore, the degree of formation permeability, k, (in combination with time and fluid type) is a determining factor in how easy initial pore fluids can be expelled during a formation history [1]. The formation permeability (controlled by size, type and connection of pores) determines the volume of retained fluid [1], which in turn controls formation porosity and pore pressure [16]. All these parameters are closely related to each other producing complex cause-and-effect relationship, among which water saturation also plays its own role.

Methods for pore pressure prediction are developed in application to normal (water bearing) shale with 100% water saturation. In shale gas formations, the water saturation can vary from small to considerable values due to gas presence [6] [7] [10]. The presence of gas brings uncertainties to log readings. Particularly, it causes the compressional velocity to decrease and resistivity to increase, and consequently influences the accuracy of conventional pore pressure estimation techniques [5].

1.3 OBJECTIVE(S) AND SCOPE OF STUDY

The objectives of this project are:

- to review the effect of gas presence and associated changes of water saturation in formation on the conventional pore pressure prediction methods;
- to suggest any modifications to workflow of pore pressure prediction;

Scope of study consists in examination of: a) mechanisms of overpressure generation and a pore pressure prediction from well logging data in offset wells for future drilling programs, b) effect of water saturation variation through the gas presence on pore pressure and its prediction technique, using books, journals and other publications. This research study is relevant because it involves the aspects that may increase the accuracy of pore pressure prediction, which is critical for designing new wells and avoiding, or at least mitigating, drilling risks. It is feasible to answer the objectives within a given timeline. Since this research study is mostly based on literature review, no hardware is needed (except personal computer with installed text editor).

CHAPTER 2
LITERATURE REVIEW

2.1 PORE PRESSURE CONCEPTS

Pore pressure or formation pressure (P_p) is defined as the pressure acting on the fluids in the pore space of a formation [1] [6]. Hydrostatic pressure (P_{hyd}) is a pressure exerted by the weight of a static column of fluid at any given vertical depth and it results from a combination of the fluid density and the vertical height of the fluid column [1] [6].

$$P_{hyd} = CF \times \rho \times g \times D \qquad \text{Eq. 2.1}$$

where ρ is a fluid density; g is an acceleration due to gravity; D is a vertical depth; CF is a conversion factor,
and in SI units the equation (1) looks like:

$$P_{hyd}\,(\text{MPa}) = \rho\left(\frac{\text{kg}}{\text{m}^3}\right) \times 9.80665\ \frac{\text{m}}{\text{s}^2} \times 10^{-6} \times \text{TVD}\,(\text{m}) \qquad \text{Eq. 2.2}$$

CF = 1

In imperial (oil field) units:

$$P_{hyd}\,(\text{psi}) = 0.052 \times \gamma\,(\text{ppg}) \times \text{TVD}\,(\text{ft}) \qquad \text{Eq. 2.3}$$

psi = lb force/in^2
$\gamma = \rho g$ is a weight density, specific weight or EqMW (ppg = lbf/gal)
weight density = [mass x acceleration due to gravity] / volume
CF = 0.052

1 ppg = 0.051948 psi/ft

Table 2.1. Conversions of pressure gradients in field and SI units [3].

Conversions	Conversions
1 g/cm^3 = 9.81 MPa/km	1 ppg = 0.051948 psi/ft
1 g/cm^3 = 0.00981 MPa/m	1 ppg = 0.12 g/cm^3
1 g/cm^3 = 1 SG	1 ppg = 0.12 SG
1 MPa/km = 0.102 SG = 0.102 g/cm^3	1 ppg = 1.177 MPa/km
1 MPa/km = 1 kPa/m	1 ppg = 1.177 kPa/m
1 g/cm^3 = 8.345 ppg	1 psi/ft = 19.25 ppg
1 g/cm^3 = 0.4335 psi/ft	1 psi/ft = 2.31 g/cm^3
1 SG = 8.345 ppg	1 psi/ft = 22.66 MPa/km
1 SG = 0.4335 psi/ft	1 psi/ft = 2.31 SG
1 SG = 62.428 pcf (lb/ft^3)	1 ppg = 7.4805 pcf

In drilling engineering, pressure gradients are more convenient to be used for determining mud weights. The pressure gradient conversions between field (imperial) and metric (SI) units are presented in Table 2.1.

Hydrostatic pressure gradient is the rate of increase of pressure due to column of fluid with depth, i.e.

$$\frac{P_{hyd}}{D}\left(\frac{psi}{ft}\right) = 0.052 \times \gamma\,(ppg) \qquad \text{Eq. 2.4}$$

The size and shape of the cross-section of the fluid column have no effect on hydrostatic pressure. The fluid density depends on the fluid type, concentration of dissolved solids (i.e., salts and other minerals) and gases in the fluid column, and temperature [4].

For a column of fresh water, the hydrostatic pressure is 0.433 psi/ft.

For water with 55,000 ppm of dissolved salts, the gradient is 0.45 psi/ft.

For 88,000 ppm of dissolved salts, the gradient is about 0.465 psi/ft [13].

Therefore, hydrostatic pressure gradient of water column is specific for a certain region and depends on the density (salinity) of formation water normal for that region [1] [6]. Normal pore pressure is defined as the pore pressure equal to the hydrostatic pressure of a column of formation water that extends to the surface [1] [6]. For instance, in the North

Sea, normal formation water density is 1.04 SG = 8.6 ppg and the normal pore pressure gradient is 0.052 × 8.66 = 0.450 psi/ft. In the Gulf of Mexico, normal formation water density is 1.07 SG = 8.94 ppg and the normal pore pressure gradient is 0.052 × 8.94 = 0.465 psi/ft [6]. Even though the pressure gradients are different, both are normal pore pressure gradients for the given regions [1] [6].

Thus, for a given region, if $P_p = P_{hyd}$, the pore pressure is normal,
if $P_p < P_{hyd}$, the formation is underpressured,
if $P_p > P_{hyd}$, the formation is overpressured.

Therefore, for any given region, knowledge of the normal fluid density and salinity is necessary. Direct measurement of the pore pressure is only possible when the formation is sufficiently permeable for the formation fluid to reach equilibrium with a pressure gauge over a short period of time [1]. Pore pressure for low permeable formations can only be estimated by indirect measurements.

According to the effective stress law (Fig. 2.1), formulated by Biot (1941) and Terzaghi et al. (1996), the overburden stress, effective stress and pore pressure can be expressed in the following form:

$$S = \sigma_e + \alpha P_p \qquad \text{Eq. 2.5}$$

where S is a vertical component of overburden stress tensor S_{ij} (vertical stress); σ_e is a vertical component of effective stress tensor σ_{ij} (vertical effective stress) exerted on grains through the grain-to-grain contact; α is Biot's poroelastic coefficient (which varies from 0 to 1, for most reservoirs conveniently assumed α=1) [3] [4]. This equation describes how the weight of the overburden is shared between pore fluid and the rock grains [6].

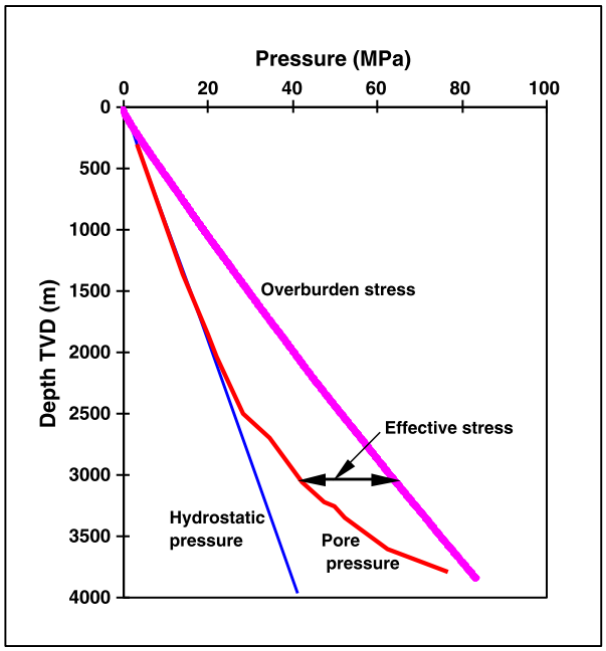

Fig. 2.1. Hydrostatic pressure, pore pressure, overburden stress, and effective stress in a borehole [3].

Overburden (lithostatic) stress (pressure) originates from the combined weight / pressure of the rock (due to grain-to-grain contact) and the interstitial fluids (water, oil, and gas) in the pore space, overlying the formation of interest [2]. Overburden increases with depth, as bulk density (ρ_b) increases and porosity (ϕ) decreases [3] (Fig. 2.2). With increasing depth, cumulative weight and compaction, fluids are squeezed out from the pore space. This leads to a proportional decrease in porosity as compaction and bulk density increase with depth. Porosity decreases exponentially with depth as effective stress on matrix increases and can be expressed by Athy type equation [3]:

$$\phi = \phi_0 \times e^{-c\sigma_e} \qquad \text{Eq. 2.6}$$

where ϕ is porosity; ϕ_0 is the porosity in the mudline; σ_e is the effective stress; c is the compaction constant in 1/m or 1/ft.

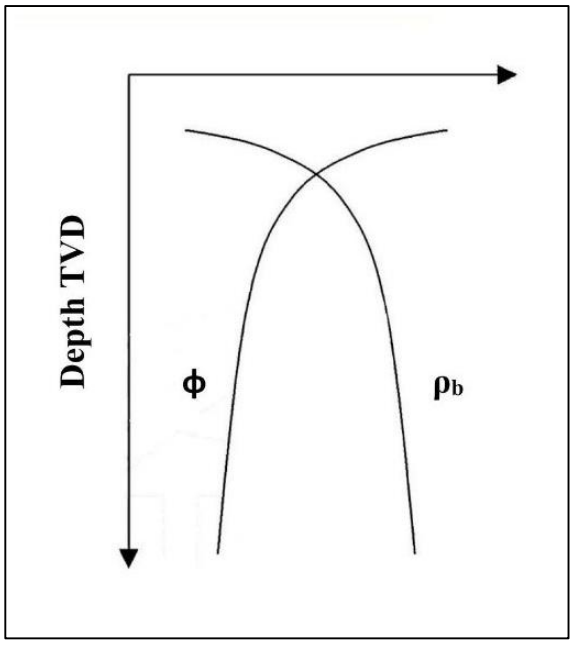

Fig. 2.2. Porosity and bulk density decrease with depth [1].

2.2 MAIN OVERPRESSURE GENERATING MECHANISMS

Formations with abnormally high pore pressures are encountered all over the world. Abnormal pressures are encountered both offshore and onshore, at deep and shallow depths, and in all types of rocks - shales, shaly sands, evaporites, carbonates, etc. from the beginning of the Paleozoic (Cambrian) to the Cenozoic era (Pleistocene) [8].

The overpressures are produced by a variety of causes, which may be physical (mechanical), chemical, or a combination of both [6]. For formations to be overpressured, they must be an isolated environments (i.e. formation is separated by impermeable barriers), or at least the fluid flow out of the formation is restricted [6]. The formation of such seal (caprock) and development of zone of abnormally high pore pressure is a highly complex mechanism. The mechanisms responsible for generating overpressures are classified into three main groups [6]:

1) Changes in rock pore volume:
    a) vertical loading (undercompaction)

b) lateral tectonic loading
c) secondary cementation

2) Changes in the volume of interstitial fluids:
   a) temperature change
   b) mineral transformations
   c) hydrocarbon generation
   d) thermogenic decomposition of hydrocarbons
   e) migration of fluids (mainly gas)
3) Changes in fluid pressure (hydraulic head) and movement of fluids:
   a) osmosis
   b) fluid pressure head
   c) oilfield operations
   d) permafrost environment
   e) differences in specific weights (e.g., between gas and oil)

Detailed description of main mechanisms is presented below.

2.2.1 Changes in Rock Pore Volume

2.2.1.1 Vertical Loading (Undercompaction)

Undercompaction of sediments is one of the major and most common occurring overpressure generating mechanisms. Sedimentation and burial processes increase the thickness of overlying sediments and consequently, the overburden pressure [1]. Increasing overburden pressure necessarily causes the simultaneous reduction of porosity and expulsion of pore fluids. Generally, a slow sedimentation rate results in a normal compaction with equilibrium between increasing overburden and reduction (expulsion) of pore fluid volume, allowing porosity to decrease [1] [6]. This normal compaction generates normal (hydrostatic) pore pressure gradient. However, if the burial is rapid and/or formation permeability is low, the fluid is not expelled at the required rate [1]. The retained fluid in the pores of the sediments becomes subjected to the load of the newly deposited

sediments, causing the pore pressure to increase (formation to be overpressured) [6]. Thus, retained pore fluid supports greater portion of overburden pressure. In this case, porosity decreases with depth less rapidly than it does under normal compaction, and such formations are called undercompacted (or in compaction disequilibrium). In other words, overpressure caused by undercompaction is recognized by higher porosity than expected at a given depth [6]. Fig. 2.3 illustrates the processes of rapid and normal burials, resulting in overpressured and normally pressured shales, respectively [9].

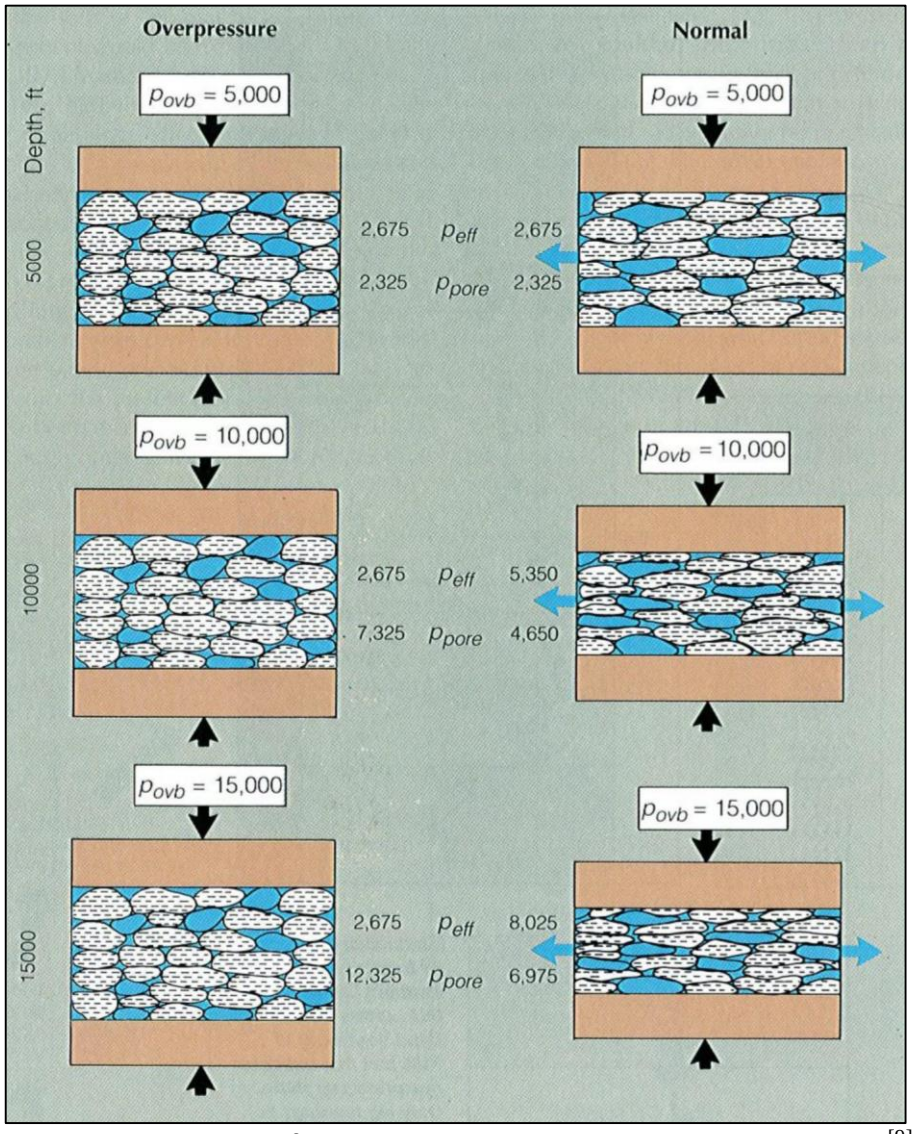

Fig. 2.3. Compaction of overpressured and normally pressured shales [9].

2.2.1.2 Lateral Tectonic Loading

Such tectonic activities as local and regional faulting, folding, lateral sliding and slipping; squeezing caused by down-dropping of fault blocks, diapiric salt, sand, or shale movements, earthquakes, etc. may lead to horizontal compression of rock and associated reduction in pore volume [6]. Uplift, faulting or folding of rocks may lead to overpressure generation through hydrodynamic activity and the alteration and redistribution of fluids and pressures [1]. Faulting may generate overpressured formations through acting as a drain (providing a conduit) or, conversely, forming an effective seal between juxtaposed permeable and impermeable layers (Fig. 2.4) [1].

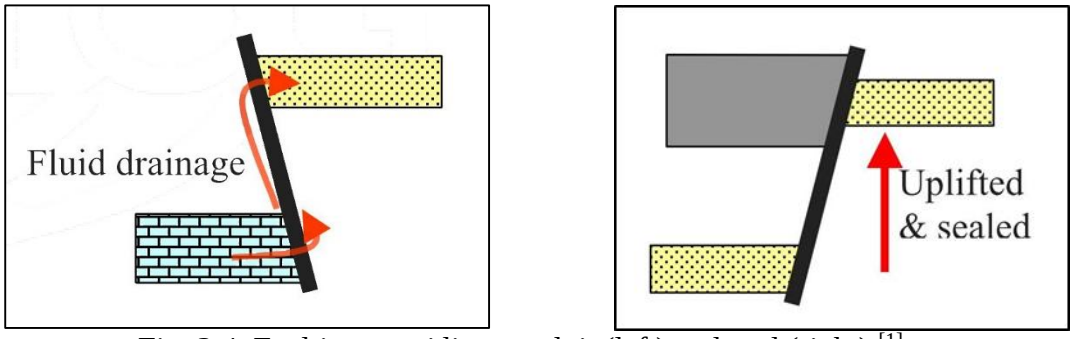

Fig. 2.4. Faulting providing conduit (left) and seal (right) [1].

Dome is a massive scale geological structure which was formed by intrusive flow of salt or shale into overlying sediments. The process of dome forming is called diapirism. Shale dome is always undercompacted and overpressured structure. Salt is completely impermeable providing perfect seals for fluid pressure (Fig. 2.5) [1] [6].

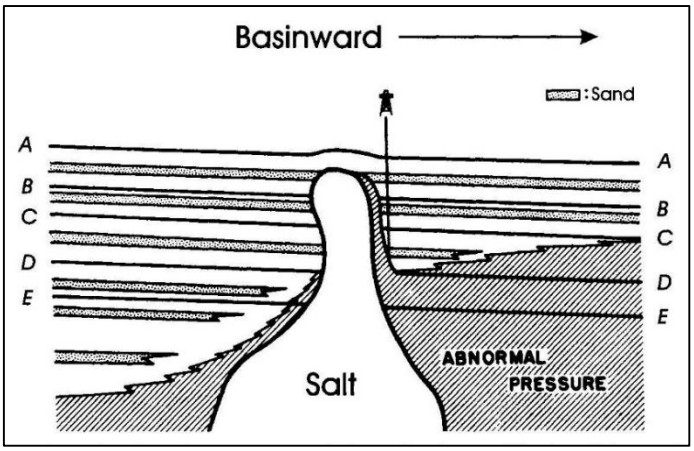

Fig. 2.5. Piercement of salt dome showing modification of abnormal pressure surface [6].

2.2.2 Changes in Volume of Interstitial Fluids

2.2.2.1 Aquathermal Expansion

The principle here is that temperature, rising with depth, heats the formation water and the latter expands; this resisted by the overburden results in increased pore pressure [1] [8]. This hypothesis has serious weaknesses: a) this would require an absolutely perfect seal, with no change in pore volume, and with no fracturing as pressure increases; such conditions are difficult to meet in real geologic setting [1] [8]; b) viscosity of heated water reduces which assists more efficient expulsion, even with low permeability [1]; c) transitional pressure increases, rather than sharp changes suggests some degree of permeability in the seal [1] [8].

2.2.2.2 Mineral Transformation (Clay Diagenesis and Gypsum Dehydration)

Diagenesis is a post-depositional mineralogical, chemical alteration of sediments with burial. The process of diagenesis is largely temperature dependent. The diagenesis of smectite (montmorillonite) to illite involves a release of lattice-bound water because illite does not have the same capacity as smectite to absorb the water. Thus, released lattice-bound water remains free and effectively causes the formation to be overpressured [1] [8]. The rate of diagenesis is also critical for overpressure generation because it must release

a lattice-bound water faster than the free water can be dissipated [8]. Similar to clay diagenesis, as gypsum transforms to anhydrite, bound water is released and able to generate overpressure if not expelled [1].

2.2.2.3 Hydrocarbon Generation

As kerogen, a source of total organic carbon (TOC) [10], passes through the so called "oil window" (certain range of depth and temperature), kerogen matures to generate oil and gas [1]. Hydrocarbon generation affects pore pressure by significant increase in fluid and pore volumes and by reduced relative permeablities to water and petroleum [8].

2.2.2.4 Decomposition of Hydrocarbons

Beyond the "oil window", at greater depths and temperatures, a breakdown of oil to lighter hydrocarbons and further thermal cracking take place [1] [6]. At higher temperatures, almost all the hydrocarbons are converted to methane. Again, this causes significant (two to three times) volume increase and results in overpressure, if the environment is sealed [6].

2.2.2.5 Migration of Fluids

In areas with lithological gaps in seals or where faults and fractured zones are present, vertical migration of fluids can be a very important and sometimes major mechanism of generation and maintenance of abnormal pressures. Upward migration of hydrocarbon gases from lower to upper horizons along high-permeability faults results in overpressure of upper horizons by piezo-convective effect [6].

2.2.3 Changes in Fluid Pressure (Hydraulic Head) and Movement of Fluids

2.2.3.1 Osmosis

In relation to possible overpressure generation, osmosis refers to the movement of water from formation containing fresh or lower saline water through a semipermeable clay or

shale to formation containing higher saline water (Fig. 2.6) [6] [1]. This movement will continue until salinities in two formations equalize. As osmosis is taking place, pore pressure decreases in less saline formation and increases in more saline one, especially when waters flows in closed compartment [1] [6]. However, osmosis is a very localized phenomenon which may occur around the salt domes and the salinity of adjacent formations and interstitial fluids is raised due to proximity to the salt [1]. Swarbrick and Osborne (1998) also stated that osmosis will not take place if shale contains microfractures [6].

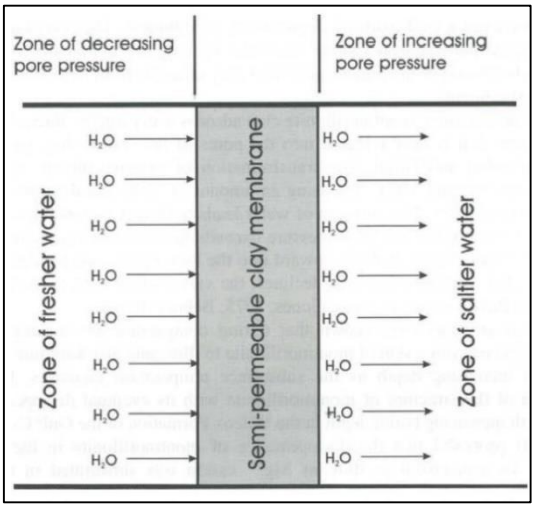

Fig. 2.6. Osmotic flow through semipermeable clay membrane (without fractures) [6].

2.2.3.2 Fluid Pressure Head

2.2.3.2.1 Piezometric Fluid Level

This mechanism involves the effect of regional potentiometric surface [6]. As an example can be an artesian water system, where a sealed reservoir type formation has an elevated water intake at surface (an outcrop) compared to the topographical elevation of the point at which formation is penetrated. Thus, the formation is overpressured due to its geometry and extended fluid column. (Fig. 2.7). Wells produce fluid to surface from such formations due to hydrostatic pressure of fluid column [1].

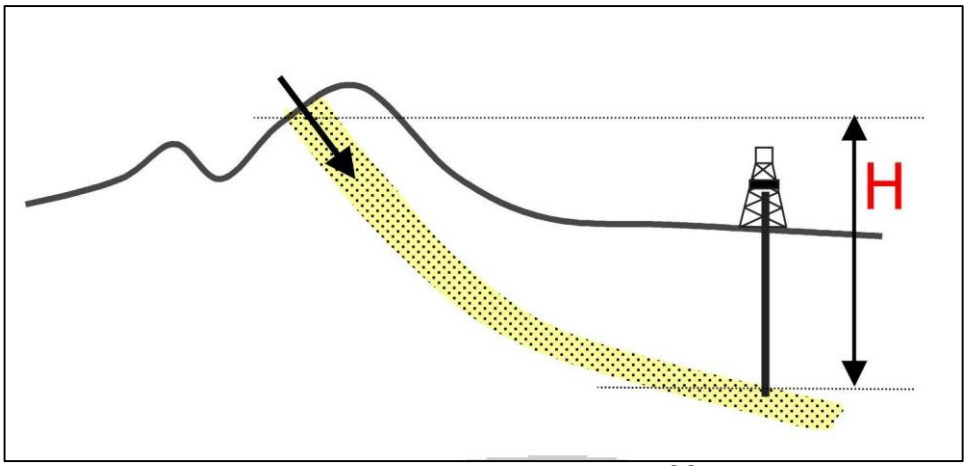

Fig. 2.7. Artesian water system [1].

2.2.3.2.2 Structure of Permeable Reservoir and Density Contrast of Fluids

In hydrocarbon reservoir structures, such as large anticlines and steeply dipping beds, overpressure exists as a result of buoyancy separation of saturating fluids due to differences between the density of oil and/or gas and that of water (Fig. 2.8) [1] [6]. The overpressure is more pronounced in the case of gas presence [6]. The differential from the normal pressure gradient depends on fluid densities and thickness of hydrocarbon column. The greatest differential is always at the top of reservoir (Fig. 2.9) [1].

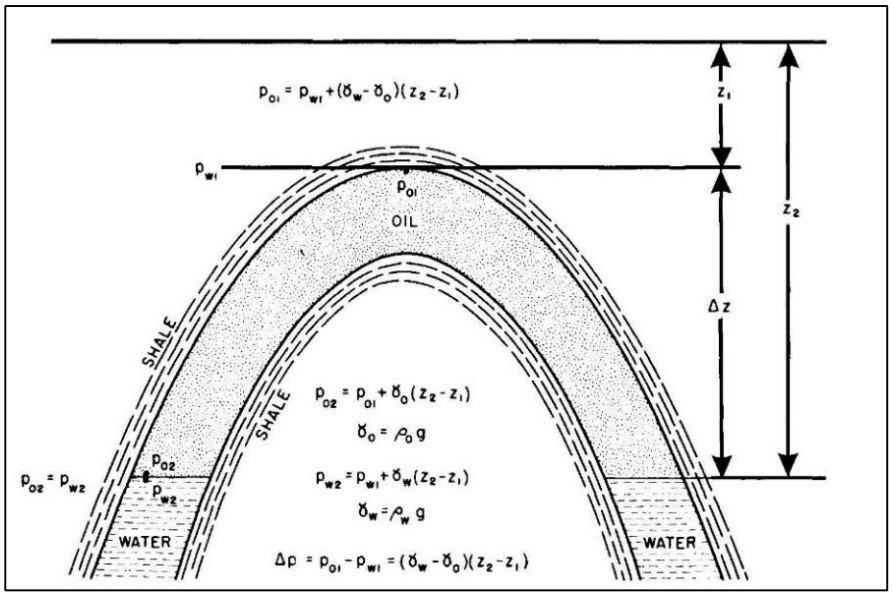

Fig. 2.8. Cross-sectional view of an anticlinal reservoir sandwiched between two impermeable shale bodies [6].

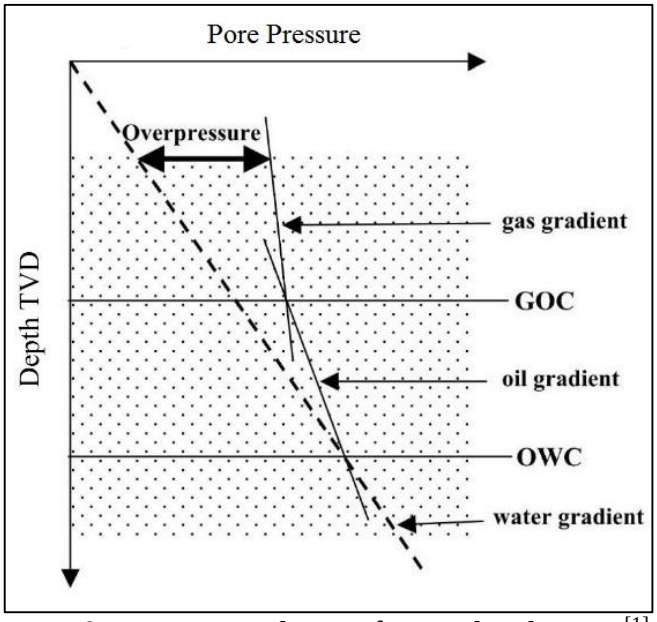

Fig. 2.9. Pressure gradients of gas, oil and water [1].

The question here is not "Which of these mechanisms is right?" but "Which of these is dominant process and under what circumstances?" [8].

2.3 WELL-LOG BASED METHODS OF PORE PRESSURE ESTIMATION

Wireline measurements from (already drilled) offset wells can be used as a source for pre-drill pore pressure prediction technique for future drilling programs [3]. Vast majority of developed methods estimate pore pressure gradients when overpressure is mainly generated by undercompaction (compaction disequilibrium) [6] [4]. Shale is known as the most sensitive lithology for compaction; "shale can be used as a geologic manometer" [6]. Undercompaction is recognized by higher porosity in comparison with a normal compaction trend [6]. Acoustic travel time / velocity and resistivity are commonly used for monitoring changes in shale porosity, and therefore detection of potential overpressure [6] [8]. For overpressure detection, the log data are plotted against depth. Under normal compaction, with constant lithology shale interval, as a porosity decreases with depth, acoustic travel time will normally decrease and resistivity will normally increase with depth. Thus, the normal trend of log measurements is interpreted as normal overburden compaction resulting in hydrostatic pressure gradient establishment over that interval. The deviation of log measurement from normal compaction trend (NCT) line refers to undercompaction and therefore, abnormally high pore pressure (Figs. 2.10, 2.11) [8] [1].

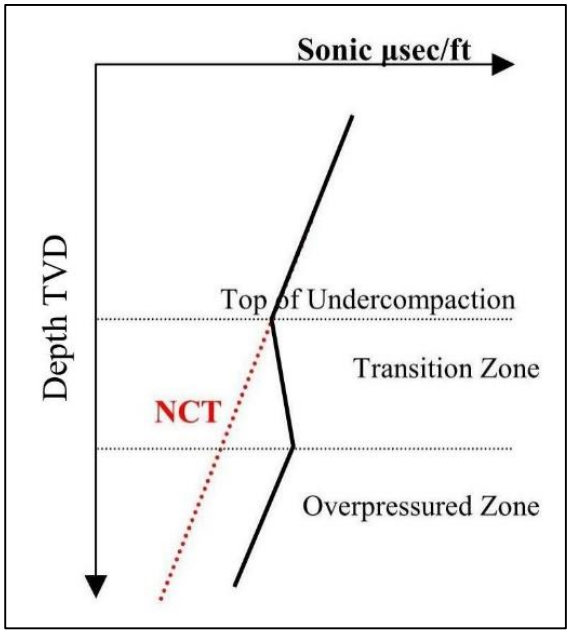

Fig. 2.10. Deviation of sonic readings from NCT [1].

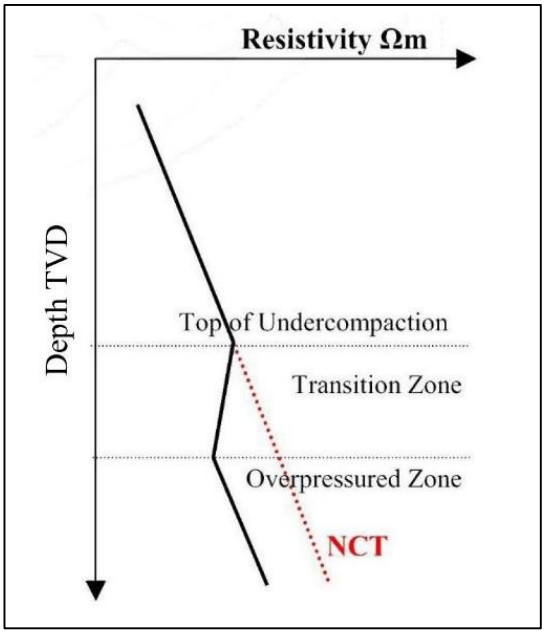

Fig. 2.11. Deviation of resistivity readings from NCT [1].

There are two general approaches for converting pore pressure indicator measurements (acoustic travel time/velocity and resistivity) into pore pressure estimates [4]:

- Direct methods
- Effective stress methods

2.3.1 Direct Methods

Direct methods relate the amount of deviation of well-log measurements from NCT (of hydrostatically pressured formation) to the observed pore pressure from adjacent formations. These methods are called direct because they require known pore pressures. There are essentially two direct methods: crossplots, first studied by Hottmann and Johnson (1965), and overlays first proposed by Pennebaker (1968) [4].

Hottmann and Johnson pioneered the pore pressure prediction from shale properties derived from well log data (acoustic travel time/velocity and resistivity). The method (based on acoustic log data) is described below and summarized in Figs. 2.12, 2.13 [14].

1) The NCT for the area of interest is established by plotting the logarithm of acoustic log readings $\Delta t_{n\,(sh)}$ from the hydrostatically pressured clean shale interval vs. depth (Fig. 2.12).
2) The same plot of $\Delta t_{ob\,(sh)}$ is made for the well in question.
3) The depth at which the plotted points diverge from the NCT refers to the top of overpressured formations.
4) The pressure at any required depth is found as follows:
    a) The divergence of observed points from the extrapolated NCT (the $\Delta t_{ob(sh)}$-$\Delta t_{n(sh)}$ values) are measured and plotted against the known pore pressures (Fig. 2.13).
    b) From Fig. 2.13 the fluid pressure gradient (FPG) corresponding to the $\Delta t_{ob(sh)}$ - $\Delta t_{n(sh)}$ value is found.
    c) The FPG value is multiplied by the required depth to obtain pore pressure.

Following these steps, a pressure gradient profile can be constructed for a well [14].

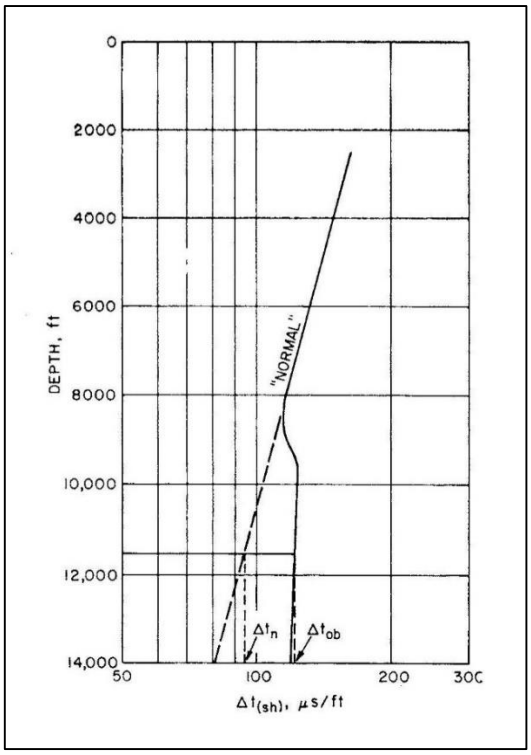

Fig. 2.12. Schematic plot of shale travel time vs. burial depth [14].

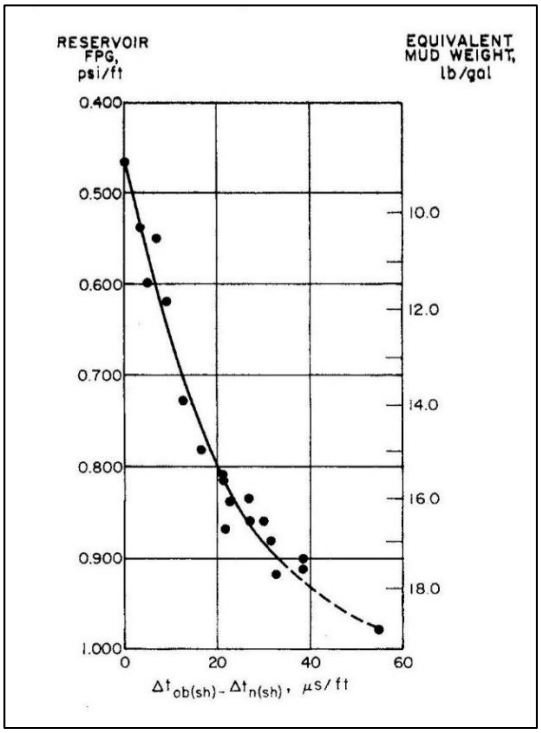

Fig. 2.13. Relation between shale acoustic parameter $\Delta t_{ob\,(sh)} - \Delta t_{n\,(sh)}$ and formation fluid pressure gradient (FPG) [14].

This method allows the interpretation of pore pressure from acoustic and resistivity measurements with an accuracy of approximately ± 0.04 psi/ft, or about 400 psi at 10,000 ft. In general, the correlations of acoustic transit time vs. depth are more easily established than the trends of shale resistivity vs. depth because less parameters influence the acoustic properties compared to the resistivity of shale. These techniques are limited to areas in which the overpressures are primarily generated by the compaction processes caused by stress of overburden [14].

Pennebaker proposed a convenient way for measuring abnormal pressures from acoustic travel time-depth plots. A transparent overlay of the lines of equal pore pressure gradient is placed over the plot and is moved laterally until the hydrostatic pressure line for the concerned area coincides with the data in the normally pressured formations just above the velocity deviation from NCT (Fig. 2.14). Pore pressure gradients are then read from overlain lines of equal pore pressure [15]. For instance, in Fig. 2.14 at 10,000 feet, the equivalent pore pressure of 18.6 ppg is estimated. The accuracy of such estimated pore pressures is within 1.0 ppg = 0.052 psi/ft, or often better, of the exact pressure. The lines of equal pore pressure gradient are calculated by Hottmann and Johnson method.

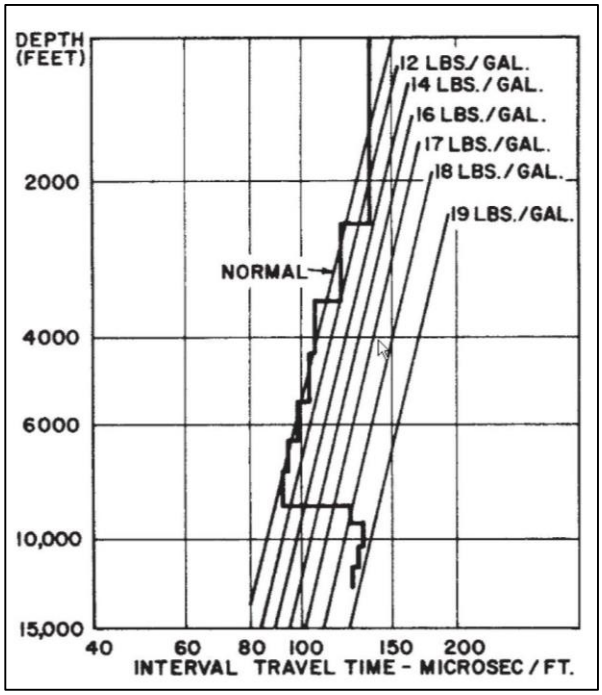

Fig. 2.14. Pennebaker overlay [15].

2.3.2 Effective Stress Methods

The fundamental pore pressure – porosity model for pore pressure prediction is based on the effective stress-porosity-compaction theory (Eq. 2.6) and Terzaghi's and Biot's effective stress law (Eq. 2.5) discussed in section 2.1:

$$\phi = \phi_0 \times e^{-c\sigma_e} \quad \text{Eq. 2.6}$$

$$S = \sigma_e + \alpha P_p \quad \text{Eq. 2.5}$$

After the rearrangement regarding pore pressure and assuming that $\alpha = 1$, Eq. 2.5 becomes:

$$P_p = S - \sigma_e \quad \text{Eq. 2.7}$$

Overburden stress (S) can be obtained from bulk density logs (ρ_b), while effective stress can be correlated to well log resistivity or sonic travel time/velocity, which are indicators of porosity [3].

These empirical methods are further classified into three categories[4]:

- Vertical methods
- Horizontal methods
- Other methods

2.3.2.1 Vertical Methods

Vertical methods, such as Foster and Whalen's equivalent depth method (1966), assume that for a given log measurement (or porosity) value, there will be a unique effective stress (or pore pressure) [4]. In other words, every point (B) in undercompacted shale is associated with a normally compacted point (A) at shallower depth [1]. The premise used here is that the matrix effective stress in the deeper abnormally pressured formation is the same as the matrix stress at the shallower "equivalent depth", because the increase in

overburden is supported by the pore fluid, and not by the matrix. Therefore, the pore fluid pressure is determined by calculating the difference between the actual overburden pressure, at the depth of interest in the abnormally pressured interval, and the matrix effective stress that exists at the "equivalent depth" of deposition [16].

These methods compute the effective stress (pore pressure) from normal compaction trend (NCT) line at the same pore-pressure indicator value as the depth of interest (Fig. 2.15) [4]. The method is expressed by equation:

$$P_p = S_B - \sigma_{e\,A} \qquad \text{Eq. 2.8}$$

$$P_p = S_B - (S_A - P_{pNA}) \qquad \text{Eq. 2.9}$$

where $\sigma_{e\,A}$ is a matrix effective stress at equivalent depth (at Point A), P_{pNA} is the normal (hydrostatic) pore pressure at Point A. S_A is the overburden stress at Point A, and S_B is the overburden stress at Point B.

$\sigma_{e\,A}$ is calculated based on the assumption that overburden pressure gradient is equal to 1 psi/ft, and on known water hydrostatic gradient for a given region (e.g., 0.465 psi/ft):

$$\sigma_{e\,A} = 1\ \frac{\text{psi}}{\text{ft}} - 0.465\ \frac{\text{psi}}{\text{ft}} = 0.535\ \frac{\text{psi}}{\text{ft}} \qquad \text{Eq. 2.10}$$

The matrix effective stress in a normally pressured section can be calculated by multiplying the matrix stress gradient by depth of Point A, as follows [16].

$$\sigma_{e\,A} = 0.535\ \left(\frac{\text{psi}}{\text{ft}}\right) \times D_A\ (\text{ft}) \qquad \text{Eq. 2.11}$$

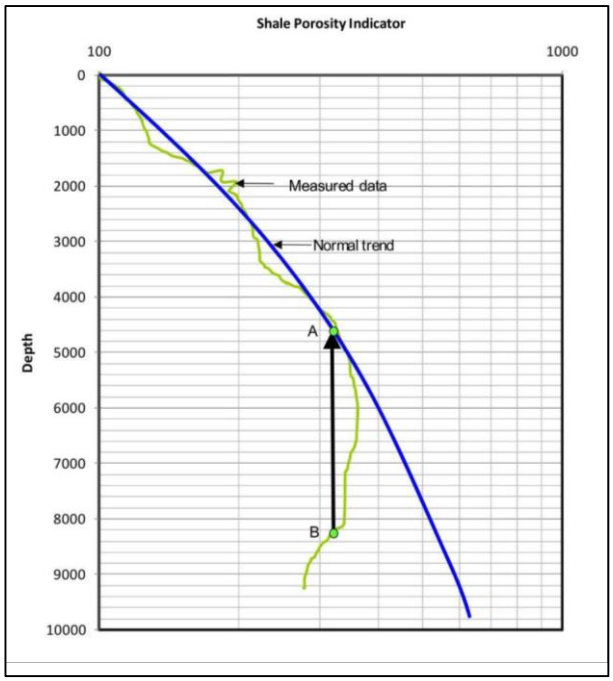

Fig. 2.15. Equivalent depth method [4].

However, the equivalent depth method is valid only over limited depths ranges because the fluid properties and lithology change with depth and causing the log measurements to change with depth even at constant porosity (effective stress) (Huffman and Bowers, 1998) [4].

2.3.2.2 Horizontal Methods

Horizontal methods, such as Eaton's method (Eaton, 1975), relates the variation of the effective stress (pore pressure) from the normal effective stress (normal pore pressure) to the deviation of a petrophysical measurement away from a NCT. These methods use an empirical relationship between pore pressure and the ratio of observed and normal well log data [4]. Eqs. 2.12 and 2.13 present the Eathon's method applied to interval transit time, and Eqs. 2.14 and 2.15 – to resistivity readings:

$$\sigma_e = \sigma_{eN}\left(\frac{\Delta t_N}{\Delta t}\right)^3 \qquad \text{Eq. 2.12}$$

or

$$P_p = S - (S - P_{pN})\left(\frac{\Delta t_N}{\Delta t}\right)^3 \qquad \text{Eq. 2.13}$$

$$\sigma_e = \sigma_{eN}\left(\frac{R}{R_N}\right)^{1.2} \quad \text{Eq. 2.14}$$

or

$$P_p = S - (S - P_{pN})\left(\frac{R}{R_N}\right)^{1.2} \quad \text{Eq. 2.15}$$

where σ_e is the effective stress, σ_{eN} is the effective stress for normal compaction at the depth of interest, Δt_N and R_N are, respectively, the interval transit time (slowness) and resistivity for normal compaction that can be obtained from the NCT, and Δt and R are, respectively, the slowness and resistivity measurements [4].

The simplicity of equations allows the Eaton's method to be applied to predict pore pressures in many regions of the world. Additionally, seismic interval velocities can be converted to interval travel times and used like acoustic log values, as well as corrected drilling exponents due to behavioural similarity of their plot to a plot of shale resistivity [16].

To evaluate the areas of application and the accuracy of these two methods, statistical analysis was performed on the data from 120 wells in three different basins: Gulf of Guinea, Angola, and North Sea (1996). The analysis showed that Eaton's method gives the best results when pore pressures are low (pore pressure gradient < 0.607 psi/ft). On the contrary, the Equivalent Depth Method is more appropriate for estimating high pressures (pore pressure gradient > 0.607 psi/ft). Moreover, the accuracy of Equivalent Depth Method depends on the accuracy of the normal compaction trend [4].

2.3.2.3 Other Methods

Later it was revealed that other mechanisms besides undercompaction (also called loading), such as aquathermal pressuring, hydrocarbon maturation, clay diagenesis, and charging from other zones (also called unloading), could contribute to overpressure generation [4].

Bowers (1995) developed a pore pressure method that accounts for both overpressure mechanisms [4]. He proposed that sonic interval velocity and effective stress have a power relationship as follows [3]:

$$V_p = V_{ml} + A\sigma_e{}^B \qquad \text{Eq. 2.16}$$

Rearranging Eq. 2.16 and considering $P_p = S - \sigma_e$, pore pressure can be obtained from interval velocity:

$$P_p = S - \left(\frac{V_p - V_{ml}}{A}\right)^{\frac{1}{B}} \qquad \text{Eq. 2.17}$$

where V_p is the compressional velocity at a given depth; V_{ml} is the compressional velocity in the mudline (i.e., the sea floor or the ground surface, normally $V_{ml} \approx 5000$ ft/s, or 1520 m/s); A and B are the calibration parameters [3]. Eq. 2.17 describes a virgin loading curve (compaction). The effective stress and compressional velocity do not follow the loading curve when formation uplift or unloading occurs (Fig. 2.16) [3]. To account for the effect of unloading curve, Bowers (1995) proposed the following empirical equation[4] [3]:

$$V_p = V_{ml} + A\left[\sigma_{max} \times \left(\frac{\sigma}{\sigma_{max}}\right)^{\frac{1}{U}}\right]^B \qquad \text{Eq. 2.18}$$

where U is an unloading parameter (a measure of how plastic the sediment is).

Rearranging Eq. 2.18 and considering $\sigma_{max} = \left(\frac{V_{max} - V_{ml}}{A}\right)^{\frac{1}{B}}$, pore pressure for unloading case can be obtained as follows:

$$P_{ulo} = S - \left(\frac{V_p - V_{ml}}{A}\right)^{\frac{U}{B}} \times \sigma_{max}{}^{1-U} \qquad \text{Eq. 2.19}$$

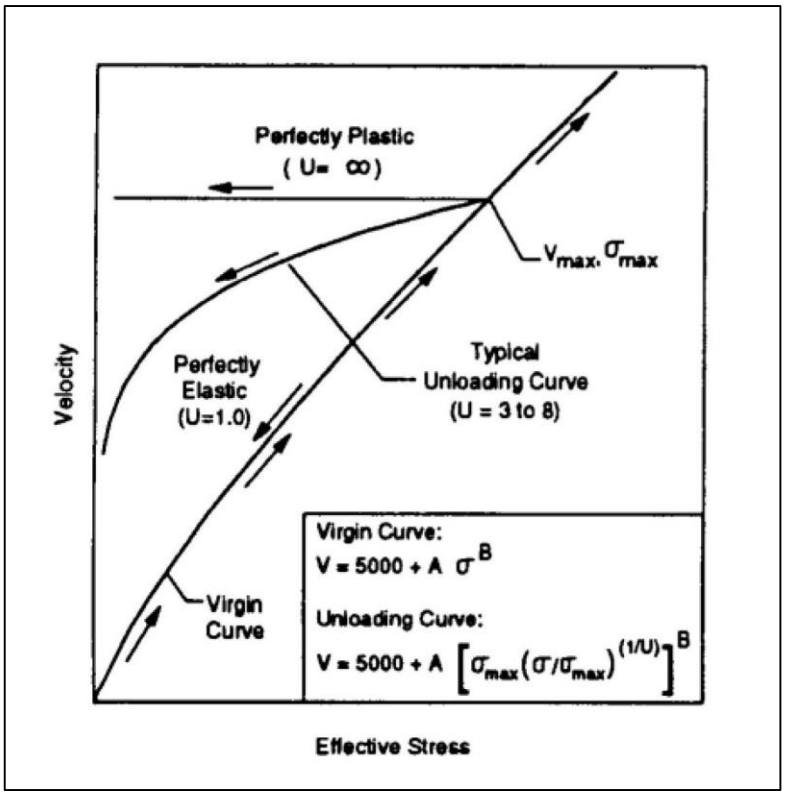

Fig. 2.16. The loading and unloading paths [4].

Two more equations allowing pore pressure estimation from acoustic logs:
Miller's sonic method [5]:

$$P_p = \sigma - \ln\left(\frac{V_m - V_{ml}}{V_m - V_p}\right) \times \frac{1}{\lambda} \qquad \text{Eq. 2.20}$$

Where V_m is the sonic interval velocity in the matrix of the shale; V_p is the compressional velocity at a given depth; and λ is the empirical parameter (normally 0.00025).

Equation proposed by Zhang [5]:

$$P_p = \sigma - (\sigma - P_N)\frac{\ln(\Delta t_{ml} - \Delta t_m) - \ln(\Delta t_{ml} - \Delta t_m)}{cZ} \qquad \text{Eq. 2.21}$$

where P_N is the hydrostatic pore pressure; Δt_{ml} is the compressional transit time in the mudline; Δt_m is the compressional transit time in the shale matrix (with zero porosity); Δt

is the measured compressional transit time; Z is the depth below the mudline; and c is the compaction constant.

As was stated before, all this well-log based pore-pressure prediction methods and algorithms are developed in application to thick and pure shale zones. For other permeable lithologies, such as sandstone, limestone, pore pressure can be predicted by assuming pressure equilibrium between shale and sandstone. However, it is not often the case in reality, because pore pressure of shale can be considerably different from the juxtaposed sandstone due to relative impermeability of shale and redistribution of overpressure within the porous and permeable sandstone. Then, centroid and buoyancy methods can be applied to estimate overpressure in non-shale formations [12] [3].

As the time passed, many Earth's regions explored and observations done, it was recognized that no unique equation/method exist, which can be applied worldwide at all times and under all conditions. This is due to facts that all methods are based to varying degrees on empirical data (Yoshida and Eaton, 1996), as well as trend line based methods have additional limitations (Dutta and Khazanehdari, 2006) [4]:

- The development or estimation of NCT may become difficult or impossible when pore pressures at shallow depths are above the hydrostatic due to rapid sedimentation, which is common in many geologic settings.
- Acoustic and pressure calibration data at shallow depths are often unavailable (due to hole size), and the determination of the normal compaction trend and subsequent pressure estimations are unreliable.
- No general rule on the shape of the NCT, which is often assumed to be a straight line in a log acoustic and resistivity vs. depth plot.
- Such trend lines cannot be transferred from one basin to another or even to different parts of the same basin without considering the geological and sedimentological history.

2.4 PORE PRESSURE PREDICTION IN SHALE GAS FORMATIONS

The contents of this section are entirely a discussion of the publication: IADC/SPE 155540. *Pore Pressure and Fracture Gradient Prediction in Shale Gas Formations: Accounting for Complex Rock Properties and Anisotropies*. Li., Sh., Purdy, P. and Wu, Sh. (2012) [5].

In unconventional shale gas formations, pore pressure can increase from normal to an abnormally high pressure over a relatively short depth interval, and its prediction offers more difficulties when compared to pore pressure estimation in normal (fully water-filled) shale. The reason for that is the gas effect on log measurements, the compressional velocity (travel time) and resistivity are particularly affected. This introduces large uncertainties on the well logging data and negatively influences the accuracy of conventional pore-pressure-prediction techniques (methods discussed in section 2.3).

Study of this gas effect on log responses, particularly on compressional velocity, was performed in shale gas formations of Bossier and Haynesville (Texas and northwestern Louisiana, USA). The Bossier and Haynesville shale is a highly productive gas shale of late Jurassic age deposited in quiet water within a restricted intra shelf (shallow ocean) basin.

The ratio of compressional to shear velocities (V_p/V_s) can be used as an indicator for the presence of gas; as the gas saturation increases, the V_p/V_s decreases. Thus, the cross-plot of the V_p/V_s ratio vs. Δt_c (or $1/V_p$) can be used to identify the gas effect on compressional velocity. As presented in Fig. 2.17, the V_p/V_s values for the gas-bearing formations (shown as red diamonds and black dots) lie lower than the V_p/V_s trend line for normal (water-filled) shale without gas effect.

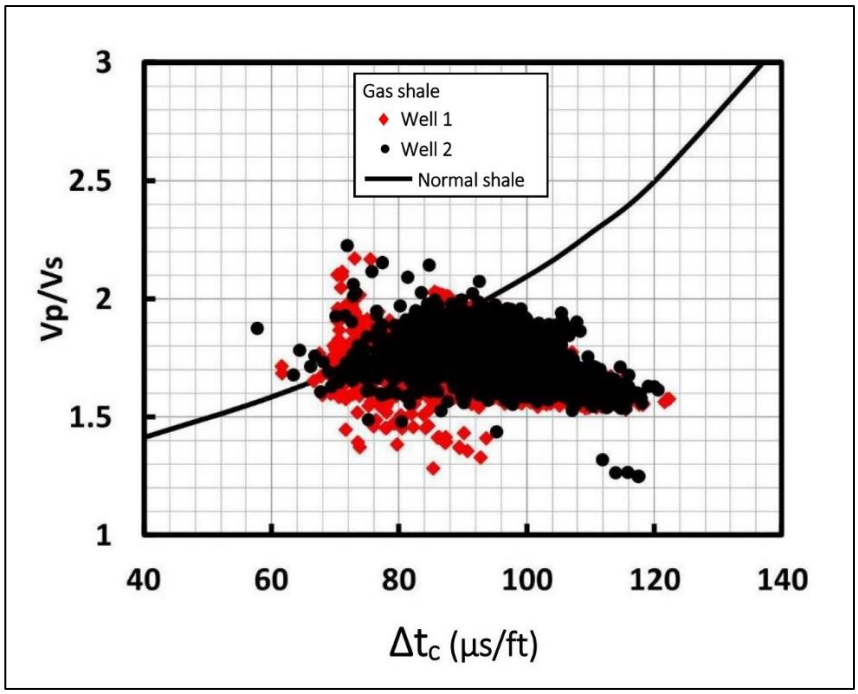

Fig. 2.17. Haynesville shale formation compared to the normal shale without gas effect (the line for the normal shale is calculated from Eq. 2.23) [5].

To perform an accurate pore pressure prediction, the gas effect on the compressional velocity (V_p) should be removed.

Castagna et al. (1985) proposed that the compressional and shear velocities in mudrocks without gas effect have a well-defined linear relationship:

$$V_p = 1.16V_s + 4461.2 \qquad \text{Eq. 2.22}$$

where V_p, V_s are in ft/sec,

or rearranging it to the following form:

$$\frac{V_p}{V_s} = \frac{1.16}{(1-0.00446\,\Delta t_c)} \qquad \text{Eq. 2.23}$$

where Δt_c is the compressional transit time in μs/ft, and V_p, V_s are in ft/sec.

Considering that $\Delta t = 1/V$, Eq. 2.23 can be rearranged regarding sonic transit time:

$$\Delta t_c = \frac{10^6}{\frac{1.16\times10^6}{\Delta t_S}+4461.2} \qquad \text{Eq. 2.24}$$

where Δt_c and Δt_s are the compressional and shear transit time in μsec/ft.

Fig. 2.18 presents the plot of Δt_c vs. Δt_s for both the shale gas formation and the normal shale (with and without gas effect, respectively). Red diamonds and black dots present the log Δt_c readings from two wells of Bossier and Haynesville shale formations, with the trend line of Δt_c values for normal shale.

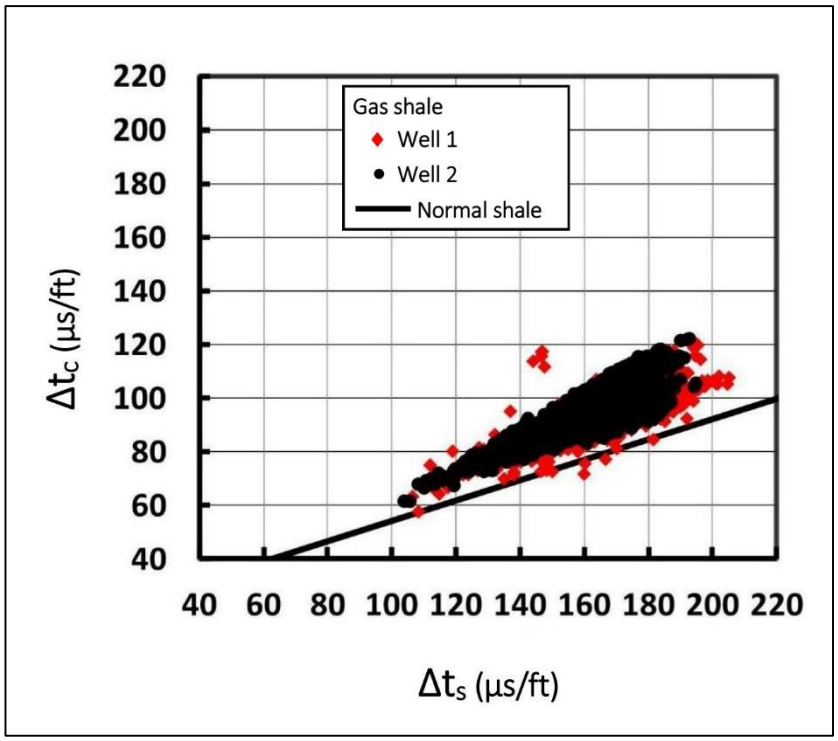

Fig. 2.18. Bossier and Haynesville shale formations compared to the normal shale without gas effect (the line for the normal shale is calculated from Eq. 2.24) [5].

It can be concluded that Δt_c in shale gas formations is much higher than the conventional shale. In other words, the V_p in shale gas formations is much lower than the conventional shale. This decrease in compressional velocity (V_p) will considerably affect the pore

pressure estimation in the unconventional shale gas formations. Therefore, before the pore pressure calculation, the V_p (Δt_c) readings, affected by gas presence, should be corrected and calculated from downhole measured V_s (Δt_s) due to its small response to gas effect (Eq. 2.22 or 2.24). After that, corrected values of V_p (Δt_c) can be used as input of one of conventional sonic methods (Eqs. 17, 20, 21).

Figs. 2.19 and 2.20 present the pore pressures calculated by Miller's method (Eq. 20) without and with gas correction to the compressional transit time (velocity), respectively.

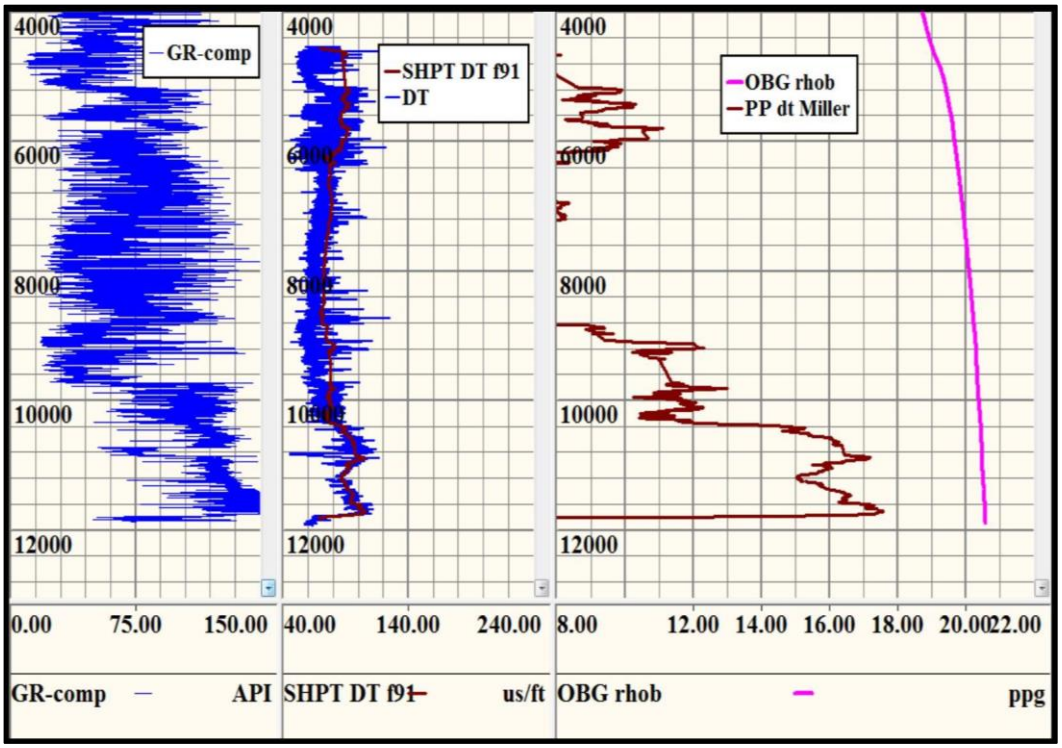

Fig. 2.19. Pore pressure calculation results from Miller's sonic method without correction of gas effect on compressional velocity [5].

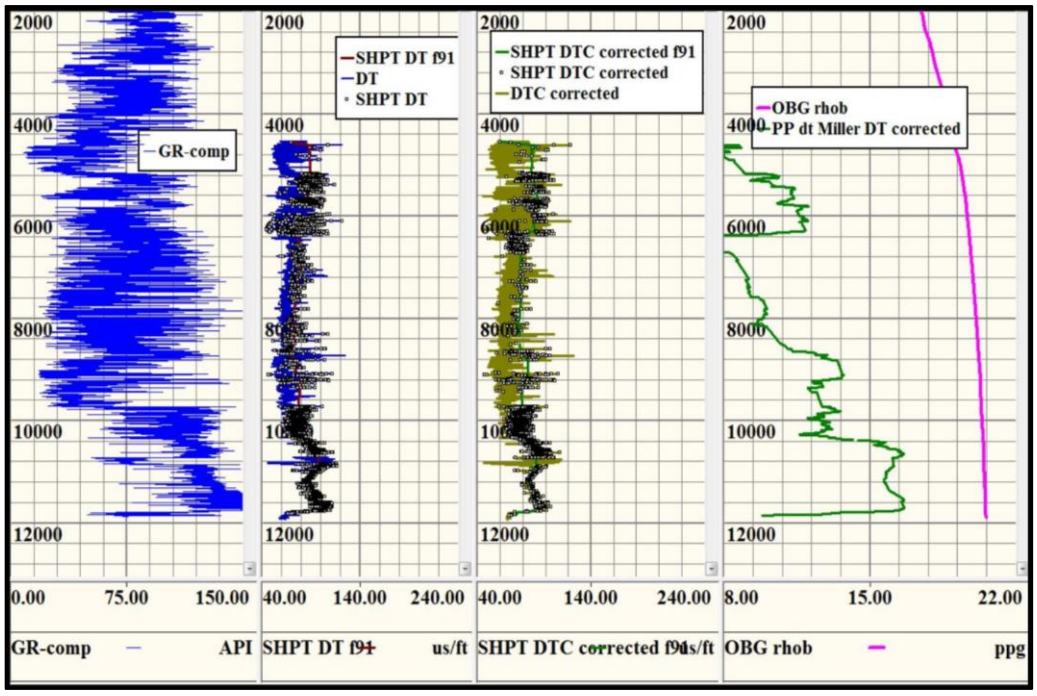

Fig. 2.20. Pore pressure calculation results from Miller's sonic method after the correction of gas effect on compressional velocity [5].

The pore pressure profile calculated using corrected Δt_c presents a good match to actual pore pressure measurements in a well (Fig. 2.20). However, the pore pressure profile calculated from uncorrected (observed) Δt_c gives poor result (Fig. 2.19). It is especially pronounced at the depth from 6,400 to 8,900 ft. (in Fig. 2.19), where the predicted pore pressure is significantly underestimated compared to real pore pressure over that section, which is in reality is normal or slightly overpressured. The drilling over this section with uncertain predicted pore pressure may result in failure. Therefore, gas correction in the compressional transit time is necessary in the gas-bearing formations. The method, using corrected compressional velocity is applicable to predict pore pressure both in shale gas formations and in gas-bearing formations in conventional reservoirs.

2.5 WATER SATURATION MEASUREMENT IN SHALE GAS FORMATIONS

Shale gas composition can be divided into kerogen and inorganic matrix. Inorganic matrix can be further divided into clay and non-clay minerals [17]. Figure 2.21 presents the petrophysical model, which can be used as a basis for understanding the structure of shale gas formations, and for visualizing total gas content estimation [17]. It is generally considered that water only exists in the inorganic matrix (Ramirez, Klein et al. 2011; Alfred and Vernik 2012; Glorioso and Rattia 2012) [17]. As shown in Figure 2.21, there are generally two types of water, clay bound water and capillary bound water.

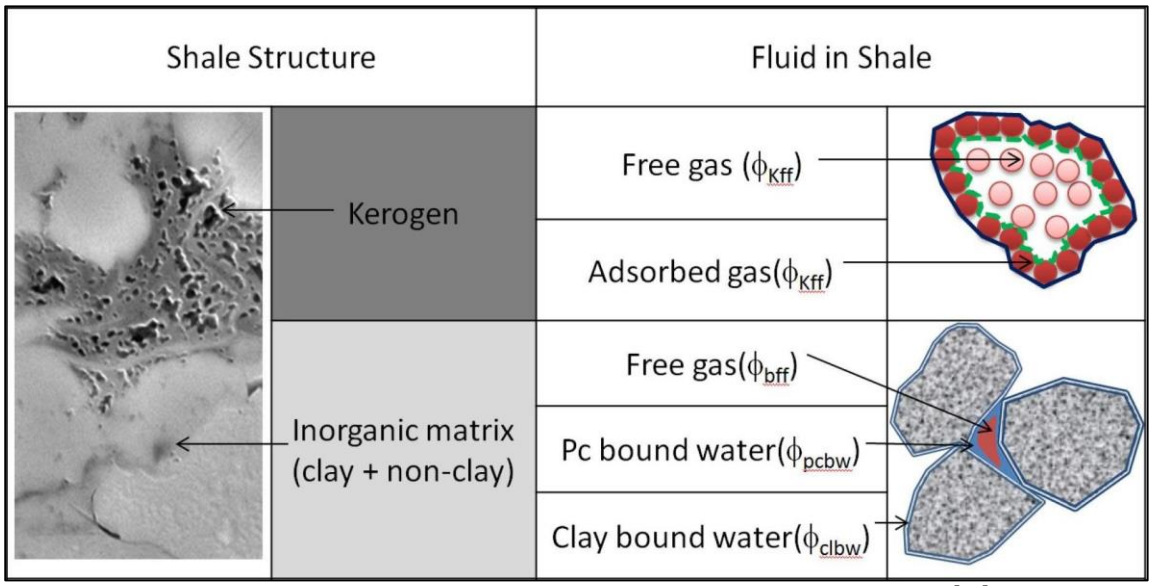

Fig. 2.21. Schematic of shale matrix and porosity composition [17].

In the laboratory, water saturation S_w is measured by standard Dean Stark or by the retort method. These methods extract fluid from crushed core samples to measure both water saturation and dry porosity. Dean Stark combines thermal and toluene extraction while retort method uses only thermal extraction. Water saturations can also be derived from well logs. Advanced logs such as NMR, geochemical and Dielectric Scanner Service [18] logs provide reliable water saturation estimation. However, due to high cost of water saturation analysis from shale coring and advanced well logs, methods to estimate water saturation based on minimum input data generally available from standard well logs have also been proposed [17]. One of such methods is discussed below.

2.5.1 Use of Pickett Plots for Water Saturation Evaluation in Shale Gas Formations

The contents of this section are entirely a discussion of the publication: SPE 146948. *Use of Pickett Plots for Evaluation of Shale Gas Formations.* Yu, G. and Aguilera, R. (2011) [19].

The method is inspired by a quick-evaluation, time-tested methodology developed by Passey et al. (1990) for shales that applies generally sonic and resistivity logs. Archie's equation was developed originally for clear sandstone reservoirs and later applied to other types of conventional reservoir rocks. Zhao et al. (2007) have shown the possibility of estimation of water saturation in shales by applying the Archie's equation. The method under discussion combines these two concepts and applies Pickett plots for quick, yet accurate, evaluation of shale gas formations from generally available sonic and resistivity logs. The major properties for evaluation of shale gas formation are porosity, water saturation, total amount of organic matter and its geothermal maturity, and the capability to flow natural gas.

Zhao and other researchers assume that Archie's (1942) equation (2.25) is applicable for estimating water saturation in shales.

$$R_t = \frac{a\,R_w}{\phi^m\,S_w{}^n} \qquad \text{Eq. 2.25}$$

where R_t is a true formation resistivity; R_w is a water resistivity at formation temperature; a is a constant (generally associated with tortuosity); m is the porosity exponent (or cementation factor), and n is the water saturation exponent (n = 2).

A sonic - porosity relationship (Eq. 2.26) was developed specifically for the case of shale formations by Magara (1978):

$$\phi = \frac{\Delta t - \Delta t_m}{B\, B_c} \qquad \text{Eq. 2.26}$$

where Δt is the sonic transit time in the formation, Δt_m is the matrix transit time of shale, B is a constant equal to 214.6 μs/ft, and B_c is a correction constant. B_c can be found from correlation of density log porosities with porosities from core analysis. For shale formation shown in Fig. 2.22, $B_c = 2.33$.

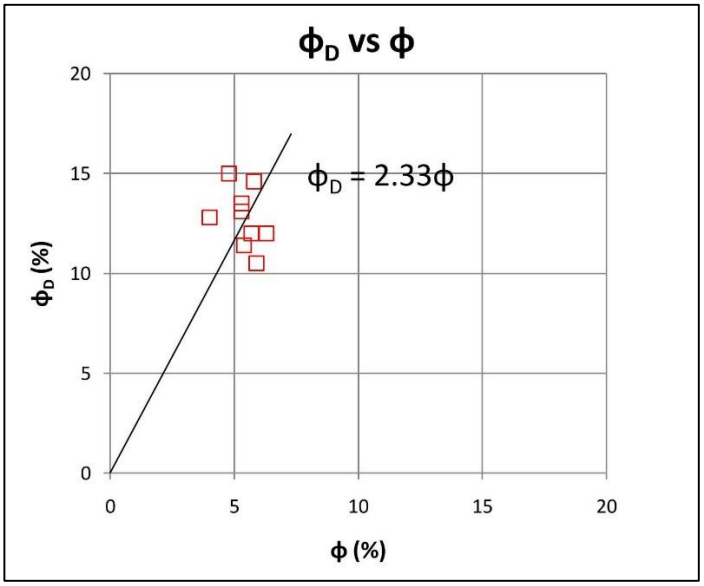

Fig. 2.22. ϕ_D calculated from density log vs ϕ measured in crushed core samples of a shale formation. Data taken from Zhao et al. (2007) [19].

Eq. 2.25 and 2.26 can be combined to obtain:

$$R_t = \frac{a\, R_w\, (B\, B_c)^m}{(\Delta t - \Delta t_m)^m\, S_w{}^n} \qquad \text{Eq. 2.27}$$

Taking logarithm of Eq. 2.27 leads to:

$$\log R_t = -m \log(\Delta t - \Delta t_m) + \log(a\, R_w) + m \log(B\, B_c) - n \log S_w \qquad \text{Eq. 2.28}$$

Assuming that there is only water in the pore space of shale (S_w= 1) and that a=1, Eq. 2.28 reduces to:

$$\log R_o = -m \log(\Delta t - \Delta t_m) + \log(R_w) + m \log(B\, B_c) \qquad \text{Eq. 2.29}$$

This theoretical relationship between resistivity and sonic transit time at 100% water saturation for a shale formation can be presented in a log-log plot, as shown in Fig. 2.23, which has the same form as the Pickett (1966, 1973) plot originally established for conventional formations.

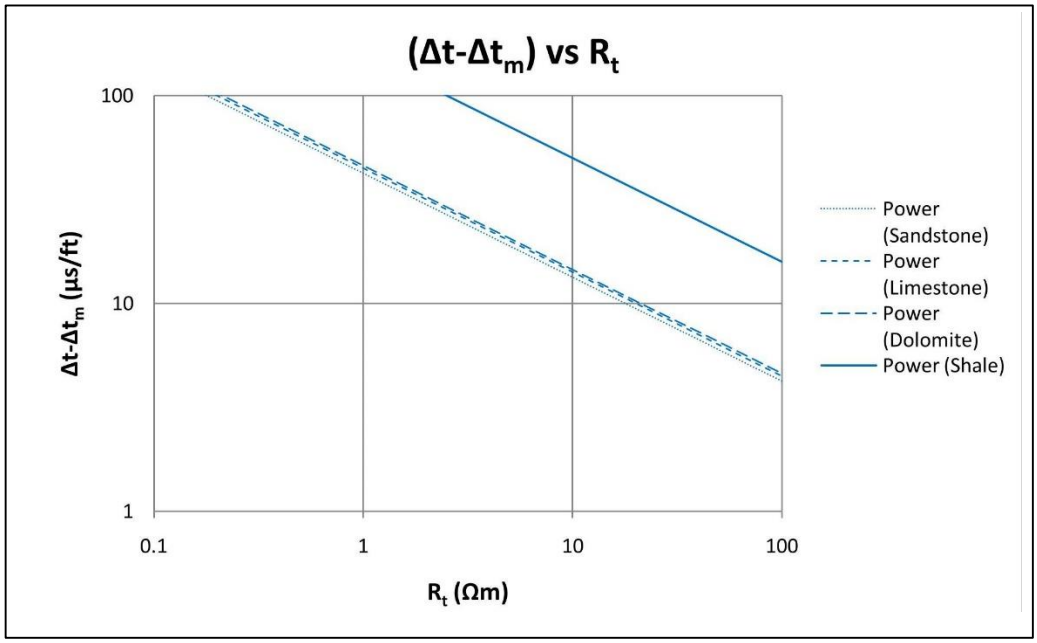

Fig. 2.23. Crossplot of (Δt - Δt_m) vs. true resistivity in a Pickett plot for shale, sandstone, limestone, and dolomite lithologies at 100% water saturation. Data are taken from Passey et al. (1990) [19].

Fore shale, here it is assumed that Δt_m = 68 µs/ft, B = 214.6 µs/ft and B_c = 2.33. Practical experience indicates that the *m* value for shale reservoirs is usually less than 2. The *m* values found for shales in the literature range from 1.45 to 1.85 (Aguilera, 1978; Zhao et al., 2007; Ramirez et al., 2011). The formation water resistivity R_w is to be corrected to the formation temperature at the depth in question (Arps, 1953; Rider, 2002).

For example, Fig. 2.24 presents the Pickett plot (ϕ vs. R_t on log-log coordinates) for Haynesville gas shale for the porosity calculated from sonic log readings (Eq. 2.26) and the true formation resistivity measured with deep resistivity tool.

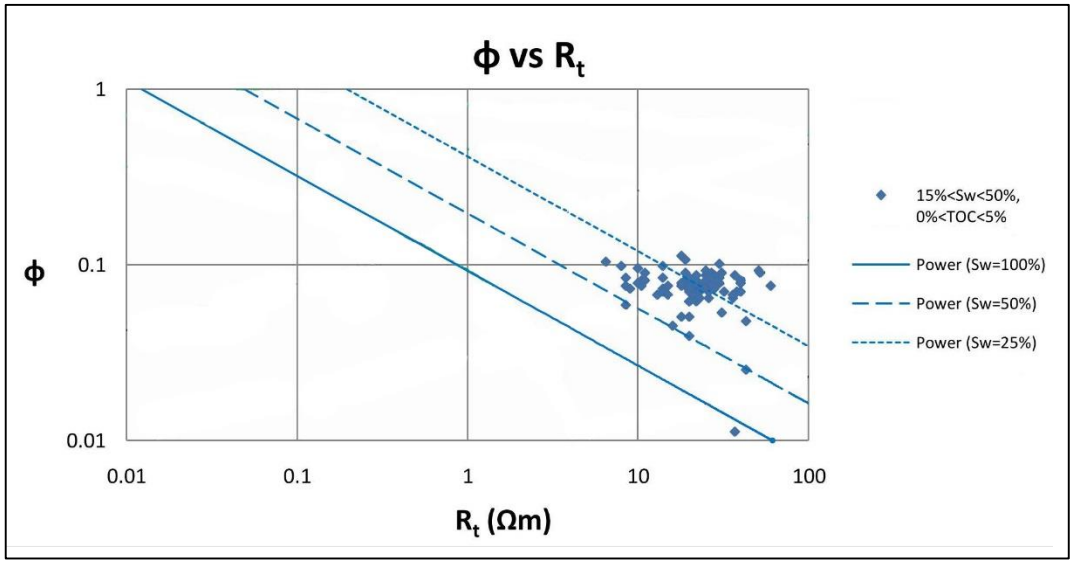

Fig. 2.24. Pickett plot for the Haynesville shale formation. Water saturation data are extracted from Ramirez et al. (2011) [19].

The set of parallel straight lines with the slope m = 1.85 represents the certain values of water saturation (100, 50, 25%) reducing upwards. The Fig. 2.24 shows that Pickett plot water saturations 15% < S_w < 50% are consistent with core data and the NMR log published by Ramirez et al. (2011).

Thus, this method using sonic and resistivity logs and integrating Archie's equation into Pickett plots provides quick and accurate estimation of water saturation in shale gas formations, as well as total organic carbon and under favorable conditions, estimates of fracture intensity and diffusion. However, the method is not meant to replace detailed mineralogical, petrophysical and thermal maturity studies of shale gas formations.

CHAPTER 3
METHODOLOGY

Steps taken to inspect correlation of water saturation (S_w) with pore pressure (P_p) are described below. The steps from no. 1 to 4 can be considered as a workflow of pore pressure prediction from sonic methods with the correction of gas effect [5] [7].

1) Since the theory of pore pressure estimation from well logging data applies to clean shale, it is critical to select pure shale for use in pore pressure analysis. Wireline gamma ray data are used to discriminate between shale and other lithologies. Shale will have high gamma ray and the points with gamma ray values less than shale baseline are not considered for analysis. Shale points defined on GR log are transferred to the corresponding acoustic log for further analysis.

2) Check the presence of gas and identify the gas effect on compressional velocity by cross-plotting V_p/V_s vs. Δt_c and comparing it with a line for shale without gas on the same cross-plot. The plot for gas-bearing zone lies below the water-filled trend line, i.e. the V_p/V_s values for gas-bearing shale are smaller than that for normal, water-filled shale.

3) If the gas effect detected, the compressional velocity V_p should be corrected and calculated from shear wave velocity (Eq. 2.22).
   If there is no gas effect on V_p, its log readings as they are can be used for further calculation of pore pressure.

4) After the treatment of sonic log readings, any existing sonic methods can be applied to calculate pore pressure in the zone of interest. It can be either Bowers method (1995)

(Eq. 2.17), Miller's method (Eq. 2.20) or an equation proposed by Zhang et al. (2011) (Eq. 2.21).

5) The next stage is an estimation of relationship between S_w and P_p (its existence and magnitude) which can be done by means of correlation analysis.

At this stage, there are two scenarios for further developments:

5.1) In case of conventional (fully water-bearing) shale, S_w equals to 100% and pore pressure can be both normal and overpressured. Therefore, correlation of water saturation with pore pressure is meaningless in such formations.

5.2) In case of shale gas formations, water saturation varies and correlation between S_w and P_p can be performed. If the correlation is significant, it is possible to find the approximating empirical equation.

S_w can be estimated from the method integrating Archie's equation into Picket plots (section 2.5.1) provided that a, m, n and R_w are constant. The a and n parameters are generally assumed to be equal 2; the water resistivity R_w is to be corrected to formation temperature; m values for shale varies from 1.45 to 1.85.

The procedure for making a Pickett plot is as follows [20]:

5.2.a) Calculate porosity ϕ from sonic logs using Eq. 2.26.

5.2.b) Plot the points of corresponding porosity ϕ and true resistivity R_t values obtained from well logs on log-log paper. Use the x-axis for the R_t scale and the y-axis for the ϕ scale.

5.2.c) Plot the corrected to formation temperature R_w value by plotting the R_w point along the R_t scale on the x-axis at the top of the graph grid where porosity is 100%.

5.2.d) Use the cementation factor m value typical for the concerned basin. Laboratory analysis is necessary for precise determination of m.

5.2.e) On a Pickett plot, the value of m determines the slope of the S_w lines. The first S_w line plotted on a Pickett plot is the 100% S_w line. To plot this line,

draw a line with a negative slope equal to m that begins at the R_w point. Use a linear scale to measure the slope.

After plotting the 100% S_w line, plot the lines representing lower percentages of S_w using this procedure:

5.2.f) Find the intercept of R_t = 1 and the 100% S_w line (made in the last procedure)

5.2.g) From this intercept, draw a line parallel to the x-axis across the plot. Any point on this line has the same porosity.

5.2.h) Where this line passes through R_t of 2, 4, 6, 8, 14, and 20, draw a series of lines parallel to the 100% S_w line.

5.2.i) Points on these lines correspond to lower percentages of S_w, calculated from the Archie equation using certain value of m and n = 2 at R_t of 2, 4, 6, 8, 14, and 20 Ohm-m.

The graphical representation of these steps (a workflow) is given in Fig. 3.1 on the next page.

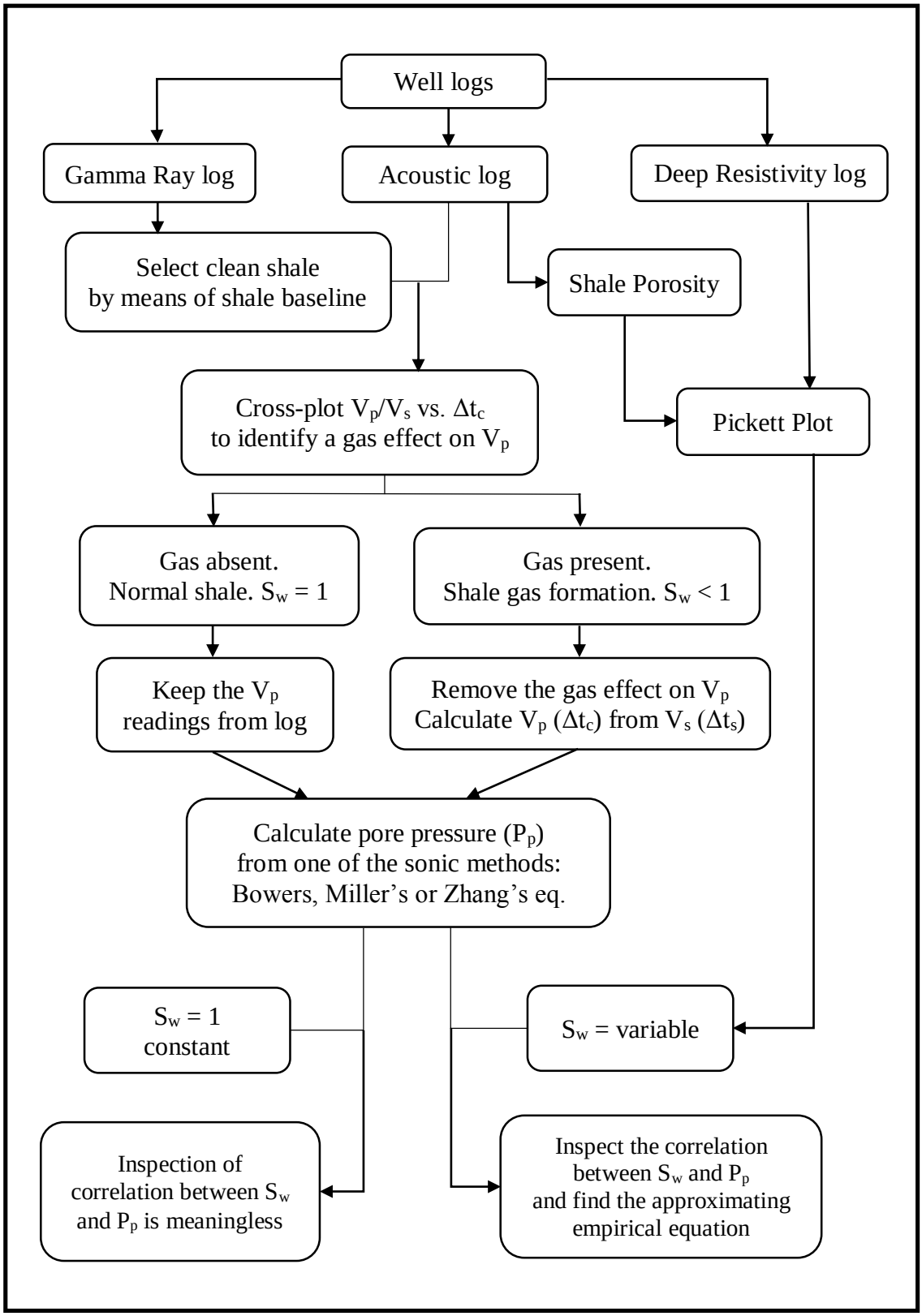

Fig. 3.1. Suggested workflow for inspection of correlation of water saturation (S_w) with pore pressure (P_p).

CHAPTER 4
RESULTS AND DISCUSSION

The contents of this chapter are essentially the speculations about the nature of fluids in shales and their effect on pore pressure estimation, and conclusion of the written materials presented in Chapter 2.

4.1 Result

After review of previous publications, it can be concluded that water saturation alteration through the gas presence in the formation does affect the pore-pressure estimation technique. However, strictly speaking, the original cause of this effect is the gas presence, and water saturation alteration is associated with a gas saturation.

4.2 Discussion

- The following two paragraphs discuss the conditions at which the water saturation does not affect pore-pressure estimation techniques:

  Water saturation is the fraction (percentage) of the pore volume of rock that is filled with formation water. It is generally assumed that the pore volume not filled with water is filled with hydrocarbons [11]. If rock does not contain hydrocarbon, water takes up all pore space, i.e. it is 100% water saturated. Despite this, as a drilling practice shows, pore pressure in such rock intervals can be both normal and abnormally high. Hereof, in fully water-bearing rocks water saturation affects neither a pore pressure, nor a technique of its prediction. However, water volume (its content) within pore space does affect the pore pressure. Indeed, the excessive volume of formation water accompanies overpressures [1] [6] [8]. It should be emphasized that conventional well-

log-based pore-pressure prediction methods and algorithms apply exclusively to thick and pure, normal (water-bearing) shale zones. For other permeable lithologies, pore pressure can be predicted by either assuming pressure equilibrium between shale and non-shale, or using centroid and buoyancy methods.

In reservoirs with abnormally high pore pressures caused by hydrocarbon generation, the fluid-pressuring phase, as it is clear from the name, is hydrocarbon. These rocks usually produce only gas or oil and gas. If water is produced from such reservoir, it usually comes from an isolated reservoir within a stack of hydrocarbon-bearing reservoir or it is mobile water from reservoir with high water content [6]. Therefore, the effect of water saturation on pore pressure in such kind of reservoir is out of question.

- The following paragraph discusses the conditions and the effect itself of water saturation variation on pore-pressure estimation techniques. Essentially, it is a conclusion of study performed by Shuling Li et al. (2012) [5] discussed in section 2.4.

  Water saturation alteration, more precisely – its reduction from 100%, might be called "conditionally and indirectly" affecting a pore pressure and its prediction technique when the porous volume is filled with both water and hydrocarbon gas. In unconventional shale gas formations, pore pressure can increase from normal to an abnormally high pressure over a relatively short depth interval due to significant increase in pore volume caused by conversion of organic material (kerogen) to gas [6]. This is how a gas presence in pore space affects a pore pressure. At the same time, the presence of gas in the shale affects log measurements. Particularly, it causes the sonic compressional velocity (V_p) to be slower / transit time (Δt_c) to increase, introducing large uncertainties and negatively influencing the accuracy of conventional pore-pressure-prediction techniques. Shear wave velocity (V_s) has a small response to gas in the pore space and can be used to remove the gas effect on the compressional velocity and correct the V_p readings. Such treatment provides a much more accurate pore pressure prediction. The method, using corrected compressional velocity, can be

applied to predict pore pressure both in unconventional shale gas formations and in gas-bearing formations in conventional reservoirs.

Fig. 4.1 summarizes the previous discussion:

In normal shale, water saturation always equals unity and it does not affect a pore-pressure estimation technique.

However, in unconventional shale gas formations, the water saturation alteration through the gas presence indirectly affects the pore-pressure estimation technique.

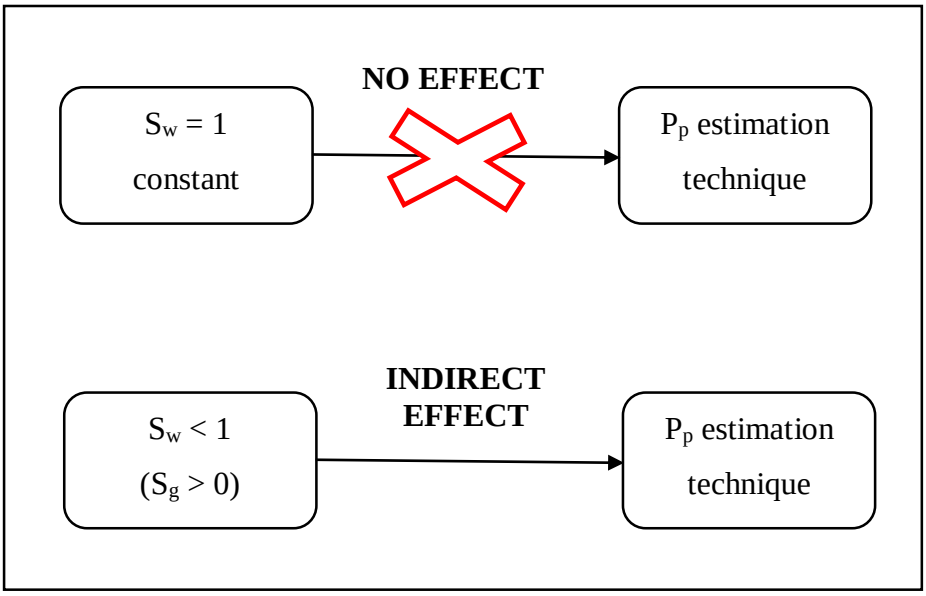

Fig. 4.1. Presence and absence of the effect on pore-pressure estimation technique.

CHAPTER 5
CONCLUSION AND RECOMMENDATION

Water saturation variation (its reduction from unity) takes place in case of other phase present in pore space. The effect of variation of water saturation on conventional pore-pressure estimation technique is pronounced through the gas presence in the formation. Thus, in normal shale, the water saturation always equals unity, and pore pressure can be both normal and overpressured, and therefore, there is no effect on P_p estimation technique from S_w variation. However, in unconventional shale gas formations, the water saturation might be moderate and high, as well as very low. Therefore, the pore pressure is usually overpressured from slightly to severely high. The gas present in shale formations slows down the compressional velocity (transit time). Consequently, the water saturation (S_w), which is associated with gas saturation as ($1-S_g$), indirectly affects the conventional pore-pressure estimation technique. As a solution, the shear velocity should be used to remove the gas effect on compressional velocity due to its low response to gas in porous medium. Removing the gas effect considerably increases the accuracy of pore pressure calculation and establishes an improved normal compaction trend line.

As a recommendation for future project work can be the inspection of correlation between water saturation and pore pressure (calculated after the correction of gas effect) in such kind of reservoir as a shale gas formation, following the proposed methodology in Chapter 3. Furthermore, a thorough study of shale gas formation in relation to its geology, more sophisticated methods of their evaluation, distribution of interstitial water and gas phases and their contribution to pore pressure would facilitate this research.

REFERENCES

1. Hawker, D. (February 2001). *Abnormal Formation Pressure Analysis.* Version 2.1, Datalog

2. Fertl, W.H., Chilingarian, G.V. (1977). Importance of Abnormal Formation Pressures. *Journal of Petroleum Technology.* 347-354

3. Zhang, J. (2011). Pore pressure prediction from well logs: Methods, modifications, and new approaches. *Earth-Science Reviews, 108.* 50-63 doi:10.1016/j.earscirev.2011.06.001

4. Tang, H. and Luo, J., Qiu, K., Chen, Yi. and Tan Ch. Ph. (2011). *Worldwide Pore Pressure Prediction: Case Studies and Methods.* Paper SPE 140954 presented at APOGCE, Jakarta, Indonesia, 20-22 September

5. Li, Sh., Purdy, C., Wu, Sh. (2012). *Pore Pressure and Fracture Gradient Prediction in Shale Gas Formations: Accounting for Complex Rock Properties and Anisotropies.* Paper IADC/SPE 155540 presented at the IADC/SPE APDTCE, Tianjin, China, 9–11 July

6. Chilingar, G.V., Serebryakov V.A. and Robertson, Jr., J.O. (2002). *Origin and Prediction of Abnormal Formation Pressures.* Developments in Petroleum Science 50. Amsterdam: Elsevier

7. Zhang, J. and Wieseneck, J., Shell Upstream Americas. (2011). *Challenges and Surprises of Abnormal Pore Pressures in Shale Gas Formations.* Paper SPE 145964 presented at the SPE ATCE, Denver, Colorado, USA, 30 October-2 November

8. Fertl, W.H., Chapman R.E., Hotz R.F. (1994). *Studies in Abnormal Pressures.* Amsterdam: Elsevier

9. Aldred, W., Bergt, D., Rasmus, J. and Voisin, B. (n.d.). Real-Time Overpressure Detection. *Oilfield Review, Drilling, 1* (3), 17-27

10. Crain (Ross), E.R. (n.d.). *Special Cases – Gas Shales.* Retrieved from http://spec2000.net/17-specshgas.htm

11. *Formation Evaluation*. (2012). Edinburgh: Herriot-Watt Institute of Petroleum Engineering Press

12. *Methods to determine pore pressure*. (2014). Retrieved from http://petrowiki.org/Methods_to_determine_pore_pressure

13. *Reservoir Engineering 1*. (2012). Edinburgh: Herriot-Watt Institute of Petroleum Engineering Press

14. Hottmann, C.E., Johnson, R.K. (1965). Estimation of Formation Pressures from Log-Derived Shale Properties. *Journal of Petroleum Technology*. 717-722

15. Pennebaker, E.S. (1968). *An Engineering Interpretation of Seismic Data.* Paper SPE 2165 presented at the SPE-AIME 43rd Annual Fall Meeting, Houston, Texas, USA, 29 September-2 October

16. Yoshida, Ch., Ikeda, Sh. and Eaton, B.E. (1996). *An Investigative Study of Recent Technologies Used for Prediction, Detection, and Evaluation of Abnormal Formation Pressure and Fracture Pressure in North and South America*. Paper IADC/SPE 36381 presented at APDTCE, Kuala Lumpur, Malaysia, 9–11 September

17. Wu, P. and Aguilera, R. (2013). *Uncertainty Analysis of Shale Gas Simulation: Consideration of Basic Petrophysical Properties.* Paper SPE 167236 presented at URCC, Calgary, Alberta, Canada, 5–7 November

18. Schlumberger. (n.d). *Dielectric Scanner Service Provides Salinity-Independent Water Saturation for Gas Shale Analysis*. Retrieved from http://www.slb.com/resources/case_studies/evaluation/dielectric_scanner_shalegas_cs.aspx

19. Yu, G. and Aguilera, R. (2011). *Use of Pickett Plots for Evaluation of Shale Gas Formations.* Paper SPE 146948 presented at SPE ATCE, Denver, Colorado, USA, 30 October-2 November

20. AAPG WIKI. (n.d.). *Pickett plot construction.* Retrieved from http://wiki.aapg.org/Pickett_plot_construction